J. Fluid Mech. (1997), *vol.* 337, *pp.* 155–191

Laboratory and numerical studies of baroclinic waves in an internally heated rotating fluid annulus: a case of wave/vortex duality?

By P. L. READ, S. R. LEWIS AND R. HIDE

Atmospheric, Oceanic and Planetary Physics, Clarendon Laboratory, Parks Road, Oxford, OX1 3PU, UK

(Received 28 March 1996 and in revised form 28 October 1996)

The structure, transport properties and regimes of flow exhibited in a rotating fluid annulus, subject to internal heating and sidewall cooling, are studied both in the laboratory and in numerical simulations. The performance of the numerical model is verified quantitatively to within a few per cent in several cases by direct comparison with measurements in the laboratory of temperature and horizontal velocity fields in the axisymmetric and regular wave regimes. The basic azimuthal mean flow produced by this distribution of heat sources and sinks leads to strips of potential vorticity in which the radial gradient of potential vorticity changes sign in both the vertical and horizontal directions. From diagnosis of the energy budget of numerical simulations, the principal instability of the flow is shown to be predominantly baroclinic in nature, though with a non-negligible contribution towards the maintenance of the non-axisymmetric flow components from the barotropic wave–zonal flow interaction. The structure of the regime diagram for the internally heated baroclinic waves is shown to have some aspects in common with conventional wall-heated annulus waves, but the former shows no evidence for time-dependence in the form of 'amplitude vacillation'. Internally heated flows instead evidently prefer to make transitions between wavenumbers in the regular regime via a form of vortex merging and/or splitting, indicating a mixed vortex/wave character to the non-axisymmetric flows in this system. The transition towards irregular flow occurs via a form of wavenumber vacillation, also involving vortex splitting and merging events. Baroclinic eddies are shown to develop from an initial axisymmetric flow via a mixed sinuous/varicose instability, leading to the formation of detached vortices of the same sign as the ambient axisymmetric potential vorticity at that level, in a manner which resembles recent simulations of atmospheric baroclinic frontal instability and varicose barotropic instabilities. Dye tracer experiments confirm the mixed wave/vortex character of the equilibrated instabilities, and exhibit chaotic advection in time-dependent flows.

1. Introduction

Baroclinic instability and the subsequent emergence of fully developed baroclinic waves and cyclones have been the subject of study for many years in the context of large-scale atmospheric and oceanic circulations (Gill 1982; Holton 1989). Such waves and instabilities form the most energetic components of the large-scale circulation in the atmosphere and oceans at extra-tropical latititudes, and they play a leading role

in the transport of heat, momentum and constituents both vertically and in latitude. A thorough understanding of their occurrence and behaviour, and the dependence of these properties on the imposed conditions, is therefore essential to any serious efforts to simulate and forecast the Earth's weather and/or the climate system.

Studies of baroclinic waves and instabilities usually take as their starting point a balanced axisymmetric (or occasionally non-axisymmetric) flow, which is then perturbed to investigate its stability. Because most studies of these processes have been stimulated by a desire to account for observations of the large-scale terrestrial atmosphere and oceans, the majority of work in this field has concentrated upon investigating the properties of baroclinic initial flows which are characterized by a *monotonic* horizontal thermal or density gradient. Such a configuration can allow the development of baroclinic instabilities in their purest form, e.g. as exhibited in the classical Eady model (Eady 1949; Gill 1982), in which wave-like perturbations grow spontaneously at the expense primarily of the potential energy stored in the initial axisymmetric or zonal flow.

Situations may arise in nature, however, where the basic thermal gradient is not monotonic, but is characterized by a local maximum or minimum of temperature on a geopotential or isobaric surface. In the terrestrial atmosphere, for example, such a configuration is often found in association with mesoscale fronts, which occur at the mature stage of development of mid-latitude cyclones. Long filaments of (usually cool) fluid with high values of potential vorticity are drawn out of the main cyclone, and find themselves surrounded by warm air of relatively low potential vorticity. Features of the opposite sign may also form in association with local diabatic heating from the release of latent heat in clouds (Joly & Thorpe 1990). Such structures may themselves be baroclinically unstable and lead to secondary development of relatively small-scale compact cyclones which can be associated with locally intense weather phenomena (e.g. Schär & Davies 1990; Thorncroft & Hoskins 1990; Thorpe & Clough 1991).

At much larger scales beyond the Earth's atmosphere, the large-scale flows observed in the atmospheres of the major planets (Jupiter, Saturn and Neptune) comprise patterns of eastward and westward jets, in which are embedded large, and apparently highly stable, oval eddies, with lifetimes of years, decades and even centuries (notably the Great Red Spot and White Ovals on Jupiter, similar spots on Saturn and the Great Dark Spot on Neptune, e.g. see Ingersoll 1990; Read 1994 for recent reviews). The zonal flows on these planets, at least above the visible clouds of ammonia and methane, are observed to be in thermal wind (geostrophic) balance with the zonally averaged temperature structure, implying that the latitudinal temperature gradient must alternate in sign in going from the equator to either pole. The apparent absence of a global equator–pole thermal contrast is generally interpreted (e.g. Ingersoll & Porco 1978) as being due to the presence of a relatively strong source of heat (associated with slow gravitational contraction and/or differential settling of constituents) in these planets' interiors, which causes the bulk of the fluid envelopes of these bodies to remain close to adiabatic. The presence of such non-monotonic thermal gradients and the associated pattern of stored potential energy has been suggested (Hide 1980; Read & Hide 1983, 1984) as one possible source of energy for the long-lived giant oval eddies on Jupiter, Saturn and Neptune, particularly given the apparent analogy between these eddies and features found in laboratory experiments on baroclinic flows in which a non-monotonic temperature gradient was imposed (e.g. Read 1986*a*; Hide, Lewis & Read 1994).

Laboratory studies of baroclinic waves and instabilities have a distinguished history

as a valuable source of insight into the fully developed forms of baroclinic flows. In the present context, laboratory studies of baroclinic flows with a non-monotonic thermal gradient include the early work of Hide & Mason (1970), who investigated the basic types of flow in a rotating annulus subject to internal heating, delineating the basic regimes of flow and the forms of the top surface flow patterns. In particular, they discovered that the form of baroclinic waves in a rotating fluid annulus, in which both cylindrical sidewalls were maintained at the same temperature with internal (ohmic) heating, took the form of chains of closed oval eddies. Ukaji (1979) later performed some similar experiments which enabled aspects of the three-dimensional structures of the regular wave regime to be determined. These experiments were pursued in more detail by Read & Hide (1983, 1984), and by Read (1986*a*), who extended the experiments of Hide & Mason (1970) to investigate a wider range of parameter space and performed some fully three-dimensional numerical simulations, mainly in the context of the proposed analogy of these waves with the giant eddies in the atmospheres of the major planets. Further aspects of the structures of these flows were also studied numerically by Read (1985, 1988), highlighting the closeness of the simulated flows to quasi-geostrophic 'free-modes' akin to adiabatic frictionless Rossby waves, zonal flows and eddies. Lewis (1992) also produced flows with many qualitative similarities to the laboratory internally heated experiments using a simplified two-level quasi-geostrophic numerical model of flow in a periodic channel.

In the present paper, we address a number of questions and issues arising from the work reviewed above. In particular, we report on a comprehensive set of laboratory experiments which further extend the work of Hide & Mason (1970) and Read & Hide (1983), in which the detailed regimes of flow in the internally heated rotating annulus, subject to cooling at both sidewalls, have been investigated, including a range of novel time-dependent and/or irregular flow regimes. The structures of the main regular flows are also studied using a high-resolution version of the Navier–Stokes numerical model used by Read (1985, 1988), in order to directly verify such model simulations against laboratory measurements. Major theoretical issues to be addressed concern (*a*) the validity of 'classical' instability theories as applied to flows in which the horizontal structure of the basic shear flow and associated thermal gradient is non-monotonic, including the applicability and relevance of the so-called 'vortex interaction' effect across a symmetric shear layer (Lighthill 1963; Hoskins, McIntyre & Robertson 1985; Schär & Davies 1990); (*b*) the extent to which the observed waves and instabilities are dominated by a barotropic or baroclinic character, given that the basic state is stably-stratified and has substantial shear in both the horizontal and vertical directions; and (*c*) the extent to which quasi-geostrophic (QG) models, such that of Lewis (1992), can capture the fully developed regimes of flow in the laboratory system.

Related to the latter point are issues such as the role of flow symmetries in determining the character of flows and bifurcations. Cattaneo & Hart (1990), for example, noted that the degree of cross-stream reflection symmetry (i.e. odd or even) of a QG zonal flow in a rectangular channel can significantly affect the selection rules for wave–wave interactions. It was suggested that this may have a strong influence on the tendency of the fully developed flow to exhibit regimes in which two or more spatially incommensurate modes are active; an issue also taken up by Lewis (1992) in relation to the odd-symmetric latitudinal structure of the zonal flows in his model. Lewis further suggested that the influence of this odd symmetry on the character of wave–wave interactions might account for the strong preference for multimode 'wavenumber vacillations' or 'interference vacillations' over single-

wavenumber amplitude modulations in his model, compared with the behaviour of the more usually considered even-symmetric baroclinic flows (cf. Pedlosky 1987).

An additional and intriguing point, also arising from barotropic and baroclinic QG models for the instability and equilibration of vorticity filaments, is the extent to which the fully developed disturbances may be regarded as waves or vortices. The tendency for the potential vorticity (PV) in the initial axisymmetric flow to 'roll up' into compact vortex-like structures raises certain expectations as to the way material fluid elements will behave in such a flow. In particular, the presence of closed PV contours would suggest that fluid may become trapped inside certain regions within the equilibrated flow, in a manner normally associated with a classical vortex. Yet the flow pattern may also behave in some respects like a classical propagating wave, with a well-defined spatial periodicity, speed of propagation, and interaction properties akin to resonant wave–wave triads (e.g. Craik 1985). In the present paper, therefore, we investigate the wave/vortex character of the internally heated baroclinic eddy flows from the viewpoint of the evolution of the potential vorticity field (diagnosed from numerical simulations), and in some dye-tracer experiments. In the latter, we try to ascertain the extent to which fluid becomes trapped for significant periods of time in the interior of such eddies, highlighting the role of time-dependence in enhancing the mixing and chaotic advection properties of the flow.

The new work builds strongly upon the earlier study of axisymmetric flow regimes by Read (1986*a*), extending some aspects of this work to baroclinically unstable regimes. Section 2 describes the experimental apparatus and numerical model, with particular emphasis on new developments since the work reported by Read (1986*a*). Section 3 outlines the basic structure of the regime diagram for this kind of flow, briefly discussing each of the main regimes of flow encountered. The structures and properties of the steady wave regime are presented in §4, for comparison with and validation of simulations using our numerical model. Time-dependent flows and regimes are discussed in §5, and results from our experiments on dye-tracer transport are presented in §6. Finally, discussion of our results and some concluding remarks are offered in §7.

2. Apparatus and models

2.1. *Laboratory system*

The apparatus used in the present study was largely as described by Read (1986*a*), and comprised two upright coaxial copper-coated brass cylinders, and a Perspex false base and lid (hereafter the 'endwalls'), both of which were horizontal and in contact with the working fluid. The working fluid itself comprised a weak electrolyte (a dilute solution of CuCl in a $\sim$ 17% mixture of glycerol in water – see later), which was placed between the cylinders, and the whole system was rotated as a rigid assembly about its axis of symmetry at angular velocity Ω, which could be varied during the experiment over the range 0.01–5.0 rad s^{-1} (though waves were typically found in the range $\Omega > 0.4$ rad s^{-1} in this series of experiments). The working fluid was heated by passing an alternating electric current through it using the coaxial cylinders as electrodes. Both sidewalls were cooled by passing water at a closely controlled temperature (typically $\pm$ 0.02 K) through water baths in contact with each boundary. The apparatus is shown schematically in figure 1, and the main dimensions and properties of the system are summarized in table 1.

Three main kinds of measurement were made in this apparatus. The heating power

Quantity	Symbol	Value	Units
Fluid depth	D	16.05	cm
Outer cylinder radius	b	10.20	cm
Inner cylinder radius	a	4.10	cm
		($\epsilon = 2.63$)	
Rotation rate	Ω	0.5–4.5	rad s^{-1}
Power input	P_0	80–350	W
Kinematic viscosity	ν	$1.62 \pm 0.02 \times 10^{-2}$	$cm^2\ s^{-1}$
Thermal diffusivity	κ	$1.31 \pm 0.01 \times 10^{-3}$	$cm^2\ s^{-1}$
Mean fluid density	ρ_0	$1.044 \pm 0.001 \times 10^{3}$	$kg\ m^{-3}$
Volumetric expansion coefficient	α	$2.90 \pm 0.02 \times 10^{-4}$	K^{-1}
Prandtl number	σ	12.4 ± 0.3	

TABLE 1. Annulus dimensions and fluid properties

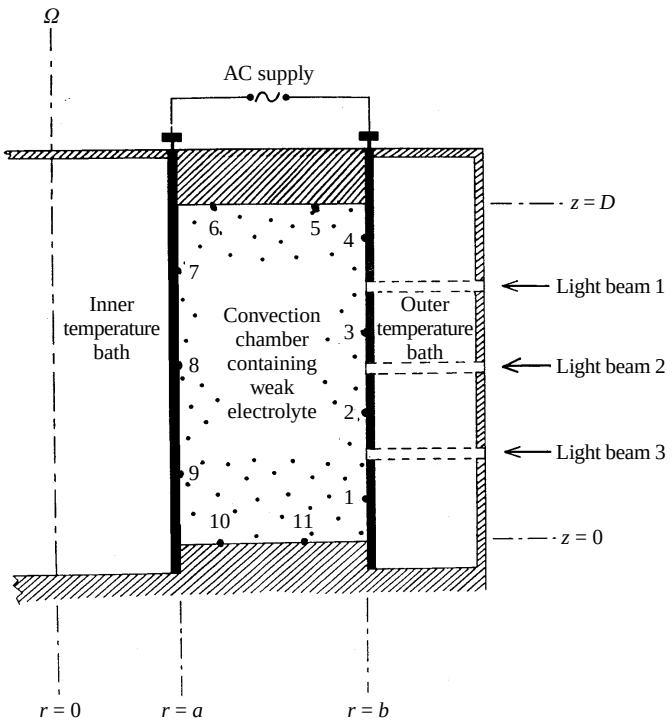

FIGURE 1. Schematic cross-section of the rotating annulus used in the present work. Locations of thermocouples to sense the boundary temperatures are indicated as numbers 1–11.

was measured to around $\pm 2\%$ using a commercial Wattmeter, which monitored the input r.m.s. current and voltage across the inner and outer cylinders. Temperatures in the sidewalls and at the upper and lower boundaries were measured using fine-wire copper–constantan thermocouples embedded in the walls and carefully insulated electrically from their surroundings. The location of the thermocouple array in (r, z) is indicated in figure 1. Horizontal velocity fields were measured in the flow using the particle tracking system described by Hignett *et al.* (1985) and Read (1986*a*). A large number of polystyrene beads (of typical diameter 600 μm) were rendered neutrally buoyant in the working fluid by adjusting the proportion of glycerol in the

mixture to match its density to that of the beads. The beads were illuminated at one of three levels in the vertical by shining a thin sheet of light (of width 5 mm) from a set of incandescent light sources through transparent windows in the outer wall and water bath. The motion of the beads in the horizontal plane was observed and measured by a closed-circuit TV camera located approximately 1.5 m above the annulus in the rotating frame, which transmitted images to a digitiser and PDP11/34 computer for analysis and display. By this means, velocity fields from tracking up to 500 beads could be either shown as streak images for qualitative display, or measured and stored for quantitative analysis using the procedures described by Hignett *et al.* (1985). Sequences of velocity fields were typically taken by measuring bead trajectories of duration 2–4 s at each of the three levels, which were cyclically switched under computer control every 10–20 s (covering all three levels in 30–60 s).

The resulting raw data comprised fields of quasi-randomly distributed horizontal velocity vectors, corresponding to each particle tracked. These data were analysed by performing a least-squares fit to a truncated series of orthogonal 'eigenfunctions' separately for each horizontal velocity component. We follow Bell (1984) in representing the entire velocity field at a given level by

$$(u,v) = \sum_{n=1}^{N} \sum_{m=0}^{M} (A_{m,n}^{(i)} \cos m\theta + B_{m,n}^{(i)} \sin m\theta) \frac{\sin n\pi x}{r^{1/2}} \tag{1}$$

where $x = (r-a)/(b-a)$ is a scaled radial coordinate, and $A_{m,n}^{(i)}$ and $B_{m,n}^{(i)}$ are regression coefficients, for which the superscript i refers to the velocity component with $i = 1$ corresponding to u and $i = 2$ to v. M and N were typically 15 and 6, respectively, compatible with the spatial resolution obtainable with the number of particles in each field. Once analysed in this form, various diagnostics of the velocity measurements could then be derived, including the computation of kinetic energy spectra, streamfunction fields etc.

Dye tracer experiments were carried out in the same apparatus, illuminating the flow from the side as in the particle-tracking experiments. The flow was visualized by injecting small amounts of a nigrosene dye from a motorized syringe pump through a fine polythene tube into a preselected point in the flow. The behaviour of the dye could then be followed on CCTV images recorded onto video tape.

2.2. *Numerical model*

The model used in the present work is essentially as described by Hignett *et al.* (1985) with modifications to include an internal heating term of the form

$$q/\mathrm{K\ s^{-1}} = \frac{P_0}{2\pi \ln(b/a) D \rho_0 c_p r^2} \tag{2}$$

(cf. Quon 1977; Read 1986*a*), where P_0 is the electrical power input (in Watts), ρ_0 is the mean density, c_p the specific heat capacity of the working fluid, and a, b and D are respectively the inner and outer radius and the depth of the annular chamber. The model uses a staggered mesh in r, θ and z as described by Hignett *et al.* (1985), stretched in r and z to accommodate boundary layers, and with a typical resolution in (r,θ,z) of $16 \times 64 \times 16$ or $24 \times 64 \times 24$ gridpoints. Boundary conditions comprise isothermal non-slip sidewalls and thermally insulating non-slip horizontal endwalls.

Simulations were typically obtained by first running an axisymmetric version of the model (cf. Read 1986*a*) to equilibrium at the required values of experimental parameters, to provide an initial balanced state for input to the fully three-dimensional

model. The initial axisymmetric state was then typically perturbed in its temperature field by addition of a localized pulse of amplitude $\sim$ 0.05–0.1 K and/or a sinusoidally varying perturbation in azimuth of similar amplitude at the centre of the channel, in order to bias the flow in favour of the preferred wavenumber, and the full model run for a further 500–2000 s (using a typical timestep of 0.02–0.05 s) until a statistical equilibrium was obtained.

3. Flow regimes and global characteristics

3.1. *Principal regimes of flow*

As discussed by various authors (e.g. Hide & Mason 1970, 1975; Read & Hide 1984; Read 1986*b*; Hide *et al.* 1994), the main regimes of flow exhibited by the internally heated rotating annulus depend strongly on the imposed experimental conditions (rotation rate and ΔT), in a manner which is similar, though (as discussed below) not identical, to the conventional and extensively studied sidewall-heated rotating annulus (Hide & Mason 1975; Hignett *et al.* 1985). Thus, at sufficiently low values of Ω and/or ΔT, the observed flow is axisymmetric, while at values greater than certain critical points the flow becomes non-axisymmetric though regular in space and steady or periodic in time, with the observed azimuthal wavenumber tending to increase as Ω increases. At the highest values of Ω and ΔT obtainable, the flow becomes progressively irregular and disordered, culminating in a fully developed state akin to 'geostrophic turbulence' (Hide & Mason 1975; Buzyna, Pfeffer & Kung 1984).

Figure 2 shows a representative set of streamfunction maps, obtained at the top level of the present apparatus using the method of Read (1989) from measurements of horizontal velocity, which illustrates the range of regular wave flows which are found in this system, culminating in a fully irregular flow (figure 2*f*). As found by Hide & Mason (1970), in contrast to the conventional sidewall-heated annulus, the regular wave flows are dominated by chains of closed gyres, which all circulate in an anticyclonic sense at this level in the vertical, typically enclosed by a continuous meandering jet stream and interspersed with weaker cyclonic circulations. Even in the fully irregular regime, the flow is still dominated by the presence of small anticyclonic gyres, which sporadically emerge, interact and decay.

3.2. *Dimensionless parameters*

By analogy with the conventional sidewall-heated annulus, the observed flow regimes may be ordered with respect to two principal dimensionless parameters, namely a Taylor number Ta, defined by

$$Ta = \frac{4\Omega^2(b-a)^5}{\nu^2 D} \tag{3}$$

(where b and a are the outer and inner radi of the annular region, D its depth and ν the kinematic viscosity), and a stability parameter or Burger number $\mathbb{B}$, defined by

$$\mathbb{B} = \frac{g\alpha\ \Delta T_z\ D}{4\Omega^2(b-a)^2} \tag{4}$$

where g is the acceleration due to gravity, α the volumetric expansion coefficient and ΔT_z the mean temperature contrast in the vertical. In practice, the latter was obtained from the mean values measured at the thermocouples in the base and lid (see figure 1). The Taylor number is defined identically to the one conventionally used in studies of the sidewall-heated annulus (e.g. Hide & Mason 1975). $\mathbb{B}$ is directly analogous

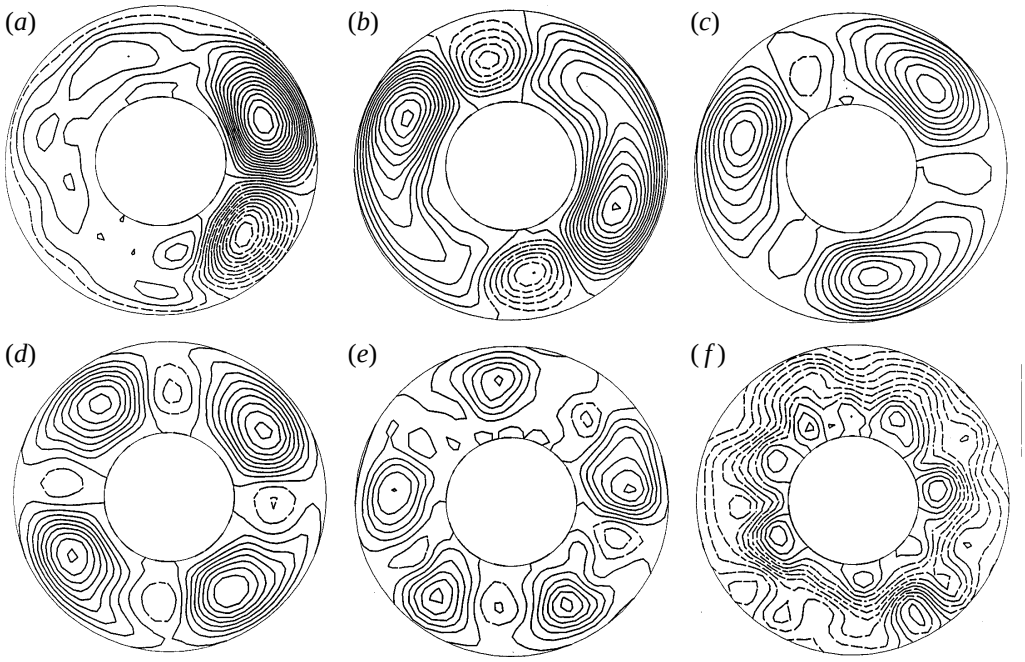

FIGURE 2. A representative sample of the range of upper-level flows obtained in the internally heated rotating annulus with cooling at both sidewalls, under various different conditions. Fields shown are streamfunction maps obtained from measurements of velocity in the laboratory at $z/D = 0.7$, and correspond to conditions: (*a*) $m = 1$, $\mathbb{B} = 1.08$, $Ta = 6.11 \times 10^6$; (*b*) $m = 2$, $\mathbb{B} = 0.444$, $Ta = 5.22 \times 10^6$; (*c*) $m = 3$, $\mathbb{B} = 0.333$, $Ta = 3.21 \times 10^6$; (*d*) $m = 4$, $\mathbb{B} = 0.127$, $Ta = 9.09 \times 10^6$; (*e*) $m = 4/5$ WNV, $\mathbb{B} = 0.0139$, $Ta = 2.68 \times 10^7$; (*f*) $m =$ irregular, $\mathbb{B} = 0.0036$, $Ta = 7.58 \times 10^7$.

to the Burger number used e.g. in quasi-geostrophic instability theory (Gill 1982; Pedlosky 1987). It is roughly equivalent to the Θ parameter (strictly $\Theta/4$) frequently defined in the context of the conventional annulus (Hide & Mason 1975), except that $\mathbb{B}$ involves the observed vertical thermal contrast whereas Θ uses ΔT impressed in the horizontal.

By systematically varying these parameters, the occurrence of different types of flow pattern can be mapped out on a regime diagram. The observed regime diagram for the present internally heated system is shown in figure 3. The numbers in each region indicate the dominant azimuthal wavenumbers m which were found in an extensive series of experiments in the laboratory. It is apparent that axisymmetric flow occurs for all values of Ta when $\mathbb{B}$ is greater than a critical value $\mathbb{B}_c$, which depends weakly on Ta itself. All flows were found to be steady unless otherwise stated, apart from a slow prograde drift of the wave pattern in azimuth. From this regime diagram, it is clear that m is a strong function of $\mathbb{B}$, with higher-wavenumber flows occurring at lower values of $\mathbb{B}$. This behaviour is consistent with the Prandtl ratio of scales $ND/fL \simeq 1$ (where N is the Brunt–Väisälä or buoyancy frequency (Gill 1982), L the horizontal length scale and $f = 2\Omega$), for which ND is approximately constant and L scales roughly as f^{-1}. Note, however, that the lowest wavenumbers ($m = 1$ and 2) only occur at relatively high values of Ta (and hence high power input and temperature contrast), in a similar way to that found in the conventional annulus (cf. figure 2 of Hignett *et al.* 1985).

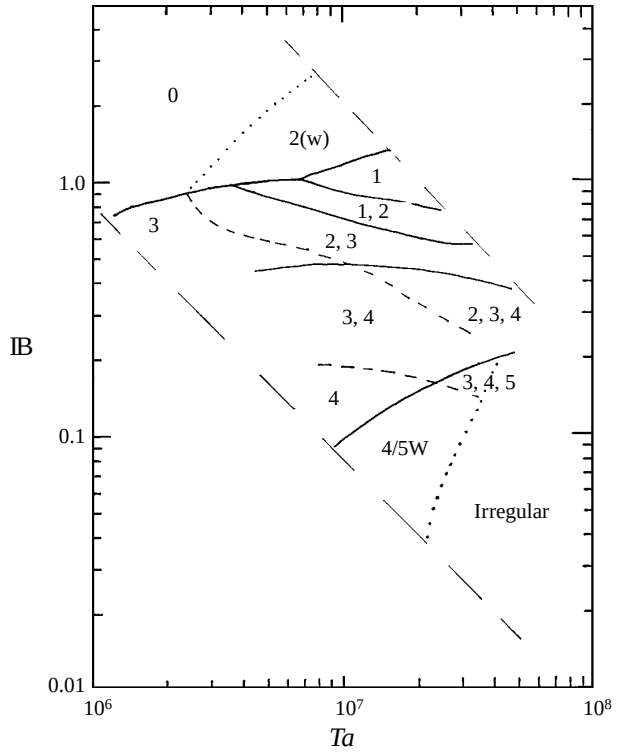

FIGURE 3. Regime diagram for the internally heated rotating annulus subject to internal heating and sidewall cooling, as a function of Burger and Taylor numbers. Numbers denote each type of wave observed in each region of parameter space. Solid lines denote well-defined boundaries observed with Ω decreasing, dashed lines denote boundaries observed when Ω increases, and dotted lines indicate the approximate location of less distinct transitions. Diagonal long-dashed lines indicated the edges of the domain explored in the present work, corresponding respectively to power inputs of approximately 30 W (lower left) and 2.5 kW (upper right).

3.3. *Multiple equilibria and vacillations*

The presence of two or more numbers in a given region in figure 3 indicates the existence of multiple equilibria, in the sense that two or more distinct steady states with different azimuthal wavenumbers could occur in the same region of parameter space. The wavenumber actually observed depends on precisely how the flow is set up and the point in parameter space is approached. From figure 3 it is apparent that multiple equilibria are comparatively common, with an increasing multiplicity of possible equilibrium states as Ta increases. The solid and dashed lines indicate the limits of a given wavenumber regime as Ω is, respectively, decreased or increased. A significant point to note is that most wavenumber states exhibit both an upper and a lower limit in IB, in contrast to the typical case in the conventional annulus, in which no firm lower limit in Θ is usually found (Hignett *et al.* 1985). This suggests that hysteresis effects associated with changes of wavenumber in the internally heated system are significantly reduced compared to conventional annulus waves.

In the same context, it is also noteworthy that time-dependent regular regimes are generally much less common in the internally heated system than for the conventional annulus, with a predominance of steady drifting wave flows. In particular, no evidence was found in the present (quite extensive) series of experiments for periodically

amplitude-modulated waves (often referred to as 'amplitude vacillation', after Pfeffer & Chiang 1967) associated with the upper range in $\mathbb{B}$ for a given wavenumber in the internally heated system, in contrast to the conventional annulus (Hignett *et al.* 1985). Close to the breakdown of regular waves into more chaotic irregular flows, however, a form of quasi-periodic or irregular oscillation in the dominant wavenumber itself is observed (hereafter termed 'wavenumber vacillation' or WNV), e.g. with intermittent exchanges between $m = 4$ and $m = 5$ around $\mathbb{B} \simeq 0.1$ and $Ta < 3 \times 10^7$. This becomes more pronounced and chaotic as $\mathbb{B}$ is decreased and Ta is increased, finally resulting in completely irregular flow characterized by a constantly varying range of relatively high dominant wavenumber patterns.

Close to the transition between axisymmetric flow and the onset of large-amplitude waves, a regime is found at large values of Ta, denoted 'W' in figure 3, in which small-amplitude waves were found which tended to be more confined in the vertical (towards the upper boundary) than in the main wave regime. This regime appears to be qualitatively similar in character to the 'weak wave' regime in the sidewall-heated annulus (e.g. Hide & Mason 1978). This regime has been commonly attributed (e.g. Hide & Mason 1978) to a weak form of baroclinic instability which owes its existence to the presence of potential vorticity gradients in the basic azimuthal mean flow. Some weak evidence for such a regime was found in the present series of experiments at high values of Ta (cf. the '2(w)' regime indicated in figure 3), where the wave/axisymmetric transition was found to be more diffuse than at lower heating rates, though the signal:noise ratio of the velocity measurements was too low to determine their structures.

3.4. *Wave drift rates*

The speed at which wave patterns drift around the apparatus is expected to be affected by the azimuthal mean flow environment surrounding the waves, both in terms of the volume-averaged azimuthal flow (effectively Doppler-shifting all wave components by an equal amount) and the mean radial gradient of background potential vorticity (possibly leading to some dispersion of different wavenumber components; cf. Bastin & Read 1997). In the present series of experiments, the volume-averaged value of azimuthal velocity v is close to zero (see Read 1986*a*, *b* and §4.1 below). Furthermore, the presence of horizontal endwall boundaries should result in relatively weak net (i.e. vertically averaged) potential vorticity gradients and hence only weak dispersion between different wavenumber components at a given point in parameter space.

Figure 4 shows a series of measurements of phase speed within the regular wave regime of the present system as a function of Ta at a constant level of heating (~ 100 W), corresponding to a mean Grashof number ($= \mathbb{B} \times Ta$) of $1.6 \pm 0.1 \times 10^6$. The phase speeds were computed from the measured drift frequencies ω_d of the dominant Fourier component in time series of radial velocity fields. The phase speed c is defined as ω_d/m, and represents the angular velocity of the wavenumber-m component of the flow in an anticlockwise sense around the apparatus. Although wave drift rates are notoriously difficult to measure reproducibly in the laboratory, Hignett *et al.* (1985) obtained reasonable agreement between (relatively non-intrusive) particle-tracking measurements and numerical simulations in their sidewall-heated experiments, in contrast to their more intrusive thermal measurements using *in situ* thermocouple arrays.

Thus, at low rotation rates in the $m = 3$ and $m = 4$ regimes, c is fairly constant around 1–2 $\times 10^{-3}$ rad s^{-1}. At higher rotation rates ($Ta > 10^7$), c tends to decrease towards zero, with perhaps a slight tendency for $c < 0$ at the highest values of Ta.

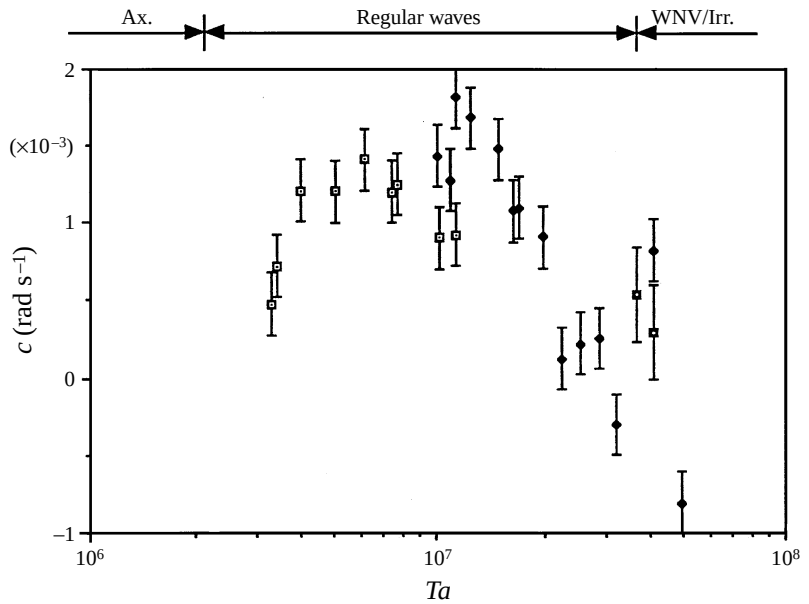

FIGURE 4. Angular phase velocity of baroclinic waves in the internally heated annulus, measured as a function of Ta at a constant value of the Grashof number $Ta \times \mathbb{B} = 1.6 \times 10^6$. Open squares denote $m = 3$, dots $m = 4$, filled squares $m = 5$.

Although there is only a narrow region of overlap in parameter space between the occurrence of two different wavenumber components, the evidence there for wave dispersion is not strong, suggesting that most of the trend in figure 4 is reflecting systematic changes in the global 'super-rotation' of the flow with Ω; a trend largely paralleled in the sidewall-heated system (cf. Read 1986*c*), where the volume-averaged azimuthal flow tends to peak at a small positive value then decay with increasing Ω. It is intriguing to note, however, that $c \sim 0$ close to both the transition from axisymmetric flow to regular waves (around $Ta \sim 2 \times 10^6$) and the onset of the multimode WNV regime (around $Ta \sim 3.5 \times 10^7$).

4. Steady wave structures and energetics

The detailed structures of flows in a rotating fluid annulus subject to internal heating and cooling at both sidewalls were discussed at some length in respect of the axisymmetric regime by Quon (1977) and Read (1986*a*), and with respect to regular wave flows in numerical simulations by Read (1985, 1986*b*, 1988) and Hide *et al.* (1994), and in laboratory measurements (in a system with a free upper surface) by Ukaji (1979). The basic axisymmetric flow in this system is clearly seen to consist of a stably stratified thermal structure with a temperature maximum at each level in the vertical close to the geometric mean radius $r = (ab)^{1/2}$. Associated with this thermal structure is a pattern of meridional flow with upwelling throughout most of the interior of the annulus (with vertical advection of temperature in approximate balance with direct internal heating) and radial motion concentrated in Ekman layers. The azimuthal flow is in approximate thermal wind balance with the thermal structure, and generally consists of pairs of oppositely directed jets at every level with cyclonic shear between them at low levels and anticyclonic shear above mid-depth. A typical

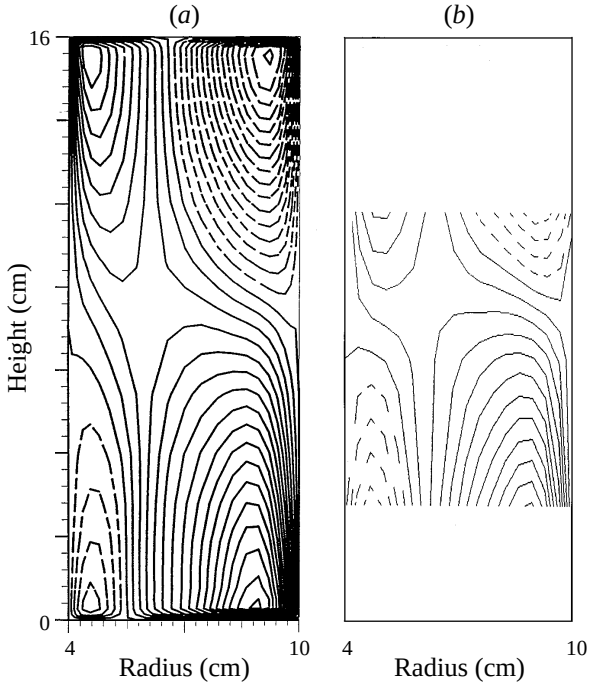

FIGURE 5. Maps in the (r, z) plane of the azimuthally averaged azimuthal flow component in a steady $m = 3$ flow in the internally heated annulus (cf. figure 2): (*a*) numerical simulation, (*b*) time-averaged laboratory measurements under approximately identical conditions. Contour interval = 0.025 cm s^{-1}.

pattern of azimuthal flow (in this case the azimuthally averaged azimuthal flow in the regular $m = 3$ regime) is illustrated in figure 5, showing a comparison between a numerical simulation and corresponding laboratory measurements (contoured from data taken at three vertical levels; cf. figure 1). The jets are generally strongest near the upper and lower boundaries with comparatively weak flow around mid-depth. The corresponding distribution of potential vorticity has an azimuthal strip of low (anticylonic) PV centred near the middle of the annular channel at upper levels, overlying a strip of high (cyclonic) PV at lower levels (e.g. see Read 1986*b*).

The structure of the eddies which form and equilibrate within the internally heated system is found to reflect the complicated thermal and PV structure of the basic axisymmetric flow. Read (1985, 1988) noted that the azimuthal phase structure of these eddies was remarkably complex, reflecting the varying baroclinicity of the background zonal flow. In particular, the eddies were found to be equivalent-barotropic (i.e. with amplitude variations but no phase variation with height) close to the 'thermal equator' (where $\partial \bar{T}/\partial r \simeq 0$), but highly baroclinic on either side of the 'thermal equator' with phase slopes of opposite sign, depending on the sign of $\partial \bar{T}/\partial r$ in the azimuthally averaged flow. Thus, although the term 'baroclinic eddy' has been in common use to describe the nature of the dominant wave-like features in this system, it is clear that the eddies combine both baroclinic and barotropic characters in a complex and unusual manner.

Such a mixed character is also a feature of the energetics of these eddies, as previously discussed in the context of numerical simulations by Read (1985, 1986*b*, 1988) and Hide *et al.* (1994). These studies computed various forms either of an

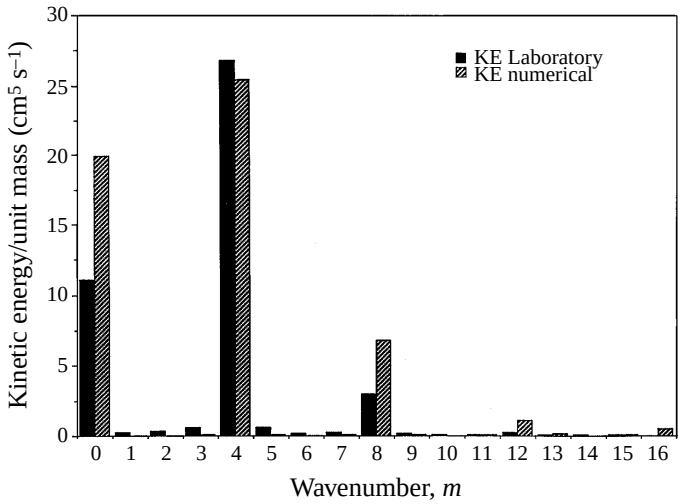

FIGURE 6. Azimuthal wavenumber spectrum of kinetic energy per unit mass from both a numerical simulation and laboratory measurements in a steady $m = 4$ flow in the internally heated annulus (cf. figure 2*d*).

approximation to the traditional Lorenz 4-box energy budget or of the Williams 3-box (Williams 1971; see the Appendix for a summary) Boussinesq energy budget (which is more accurate for the present system) for the equilibrated regular wave flows in the internally heated annulus. These calculations showed that the maintenance of the eddy kinetic and available potential energies were dominated by the classical baroclinic terms, even though eddy momentum fluxes and the lateral shear of the mean zonal flow component were non-negligible.

In the present section, we carry out a direct quantitative comparison between laboratory measurements in the steady wave regime of the internally heated system and numerical simulations using our three-dimensional Navier–Stokes model. The simulated flow structures were compared with laboratory measurements of horizontal velocity in two typical cases of regular $m = 3$ or 4 flow.

4.1. *Kinetic energy spectrum*

As apparent in the overview figure 2, the regular wave regime typically comprises a symmetric train of closed eddies with a well-defined dominant wavenumber. The discrete nature of the wavenumber spectrum is clearly evident in the amplitude and kinetic energy spectra obtained in this regime, an example of which is illustrated in figure 6 for a regular steady $m = 4$ flow. The laboratory spectrum is computed from measurements of horizontal velocity at each of the three levels sampled in the vertical, and integrated with respect to volume over the entire domain of the annulus using a form of Simpson's rule to give a measure of the total kinetic energy ($\simeq (u^2 + v^2)/2$) in each of the azimuthal Fourier harmonics included in the velocity interpolation procedure. Also shown are results from a numerical simulation carried out under as closely similar conditions to the laboratory experiment as possible, in which the total kinetic energy is also integrated over the whole volume of the annulus.

Both laboratory and numerical spectra clearly comprise a mean zonal component ($m = 0$), the wavenumber $m = 4$ and its harmonics, with very little energy in any of the non-harmonic components. The small amount of energy in non-harmonic components present in the laboratory spectrum is attributable largely to measurement

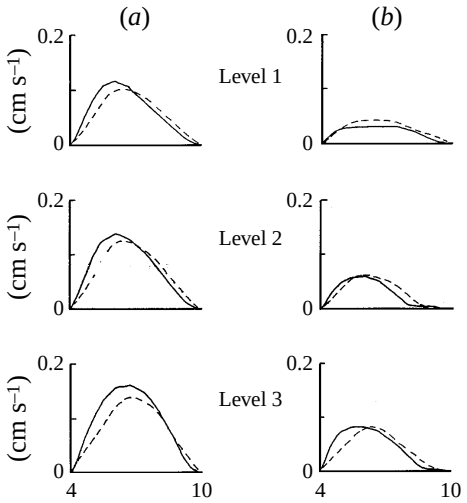

FIGURE 7. Radial profiles of the amplitude of radial velocity in the form of azimuthal Fourier components at the three levels measured in the laboratory for a steady $m = 3$ flow in the internally heated annulus (cf. figure 2*c*): column (*a*) $m = 3$ and (*b*) $m = 6$. Solid lines denote results from the numerical simulation and dashed lines show interpolated measurements of velocity in the laboratory.

noise and calibration errors in the velocity measurements. Very little energy is present in these components in the numerical simulation. Quantitative agreement between the numerical simulation and the laboratory measurements is relatively good (i.e. within 4%) for $m = 4$, but rather poorer for the harmonic components and $m = 0$. This is almost certainly due to the inadequate sampling of the wave and zonal flow structures in height by the laboratory measurements, which only really cover around 50% of the depth of the annulus. In particular, as figure 5 illustrates, the laboratory measurements miss the strongest regions of zonal flow for $z > 11.5$ cm and $z < 3$ cm, leading to a serious underestimate of the total kinetic energy for $m = 0$. Likewise, the measurements also miss a significant region of enhanced wave amplitude at $m = 8$ and $m = 12$ in the upper regions of the flow, which are clearly seen in the numerical simulations. Figure 5 does indicate, however, that laboratory measurements and numerical simulations agree to within a few per cent at the locations where measurements are made, and this point is further apparent in a comparison of wave amplitude and phase structures.

4.2. *Wave amplitudes and phases*

From an azimuthal Fourier analysis of the results of the numerical simulations, the detailed spatial structure of each azimuthal wave component within the equilibrated flow could be analysed and interpolated to the location of the laboratory velocity measurements. Figures 7 and 8 show radial profiles of the amplitude of the radial and azimuthal (zonal) velocity Fourier components respectively for the $m = 0$ azimuthal mean flow (zonal velocity only), the dominant wavenumber and its first harmonic, this time from a steady $m = 3$ flow in the internally heated annulus (results for the $m = 4$ case are very similar). The solid lines show the profiles analysed from the numerical simulation (with a resolution of 16×16 in (r, z)), and the dashed lines show the profiles obtained from the interpolated velocity measurements in the laboratory.

Profiles of radial velocity (figure 7) show generally good agreement in amplitude between measurement and simulation. Some systematic differences are apparent,

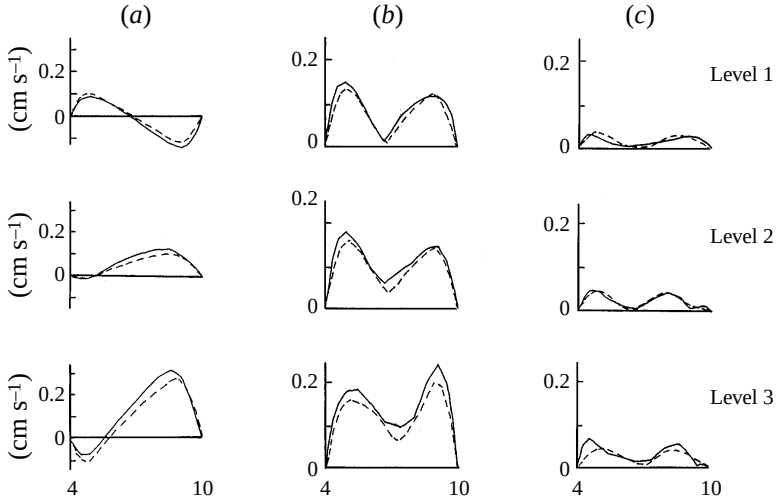

FIGURE 8. As figure 7 but for radial profiles of azimuthal velocity components: column (*a*) mean azimuthal flow ($m = 0$), (*b*) amplitude of the $m = 3$ and (*c*) amplitude of the $m = 6$ components.

however, with a noticeable tendency at all levels for the amplitude in the simulation to exceed that of the measurement. In addition, the centroid of the measured amplitude profile tends to lie closer to mid-radius than that of the simulation. The latter trait may reflect a genuine systematic difference, though could also reflect to some extent the limited truncation of the function series used to interpolate the laboratory measurements, and also the choice of radial eigenfunction (see equation (1)) which may not be as well suited to representing certain features in cylindrically curved domains as e.g. Bessel functions (though the latter are much less convenient computationally).

Measured azimuthal velocity amplitude profiles (figure 8) are generally close to the simulated profiles, with little evidence for systematic differences in their shapes. Indeed the measured profiles reveal considerable detail at small scales, especially in the harmonic $m = 6$ component, which is closely reflected in the simulated profiles. The close agreement in amplitude of the $m = 0$ component between simulation and measurements is clearly shown in figure 8(*a–c*), though with a small difference in the location of the zero-velocity line between the two cases.

The azimuthal phase structure of the dominant $m = 3$ wave component is illustrated in figure 9, which shows radial and vertical profiles of relative phase of the radial velocity component at two radii and two heights respectively in the flow discussed above. In the case of both the simulation and the measurements, phases have been measured with respect to mid-radius at the top level of the measurements (at $z = 11.2$ cm) for ease of comparison. The continuous profiles are taken from the simulation, while the measured phase points are plotted as discrete points with error bars at the equivalent heights or radii. The simulated profiles in figure 9 clearly show the pronounced phase tilts with radius and height within each eddy, with a clear tendency for the $m = 3$ component to lean in opposite senses with height on either side of $r \simeq 5.0$ cm.

The vertical profile at $r = 5.0$ cm in figure 9(*a*) indicates almost no phase tilt with height in the main body of the flow (also reflected in the measurements to within the phase error of $\simeq \pm 0.05$ rad), except in the vicinity of the Ekman layers close to the

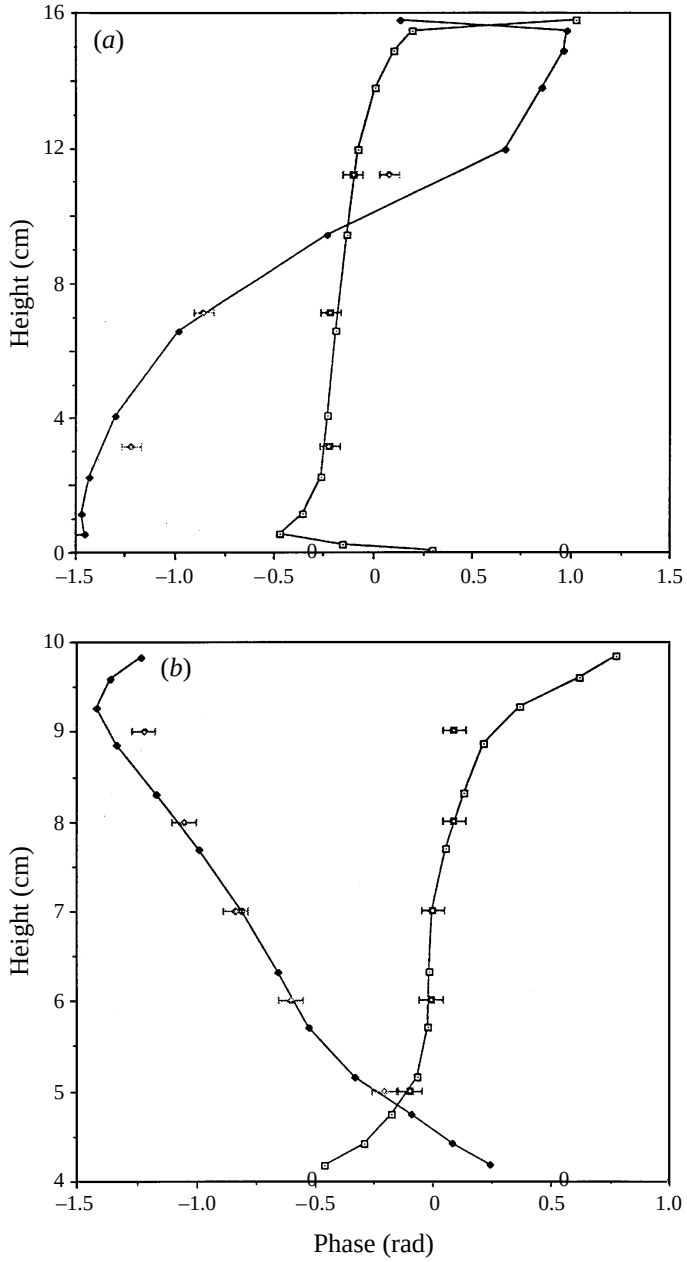

FIGURE 9. Profiles of the relative variation of the azimuthal phase of the $m = 3$ component in a steady $m = 3$ baroclinic wave in the internally heated annulus (cf. figure 2*c*): (*a*) vertical profiles at $x = (r-a)/(b-a) = 0.167$ (filled points and diamonds) and $x = 0.833$ (open points and squares); (*b*) radial profiles at $z/D = 0.7$ (open points and squares) and $z/D = 0.2$ (filled points and diamonds). Continuous lines represent results from the numerical simulation and laboratory measurements are shown as discrete points with error bars. Phase is measured with respect to $x = 0.5$ at $z/D = 0.7$ for ease of comparison between laboratory and numerical simulation.

horizontal boundaries. The phase tilt nearer the outer cylinder shows a steep increase of phase with height over a range of more than 2 rad, at a radius at which the mean flow is strongly baroclinic. In this case, the measurements suggest a somewhat lesser slope with height than the simulation, though this may again reflect systematic errors in the interpolation method.

The radial profiles in figure 9(*b*) show generally good agreement between simulation and measurements within the central part of the annular channel, where the signal:noise ratio for amplitude measurements is best, though with some increasing differences appearing as the sidewalls are approached. The simulated profiles show clear evidence for a modification of the phase structure in the vicinity of the viscous sidewall boundary layers (of thickness $O((\nu/\Omega)^{1/4}) \simeq 0.5$ cm), which the velocity measurements are unable to resolve accurately.

5. Time-dependent flows

In this section we discuss various aspects of time-dependent baroclinic flows in the internally heated annulus. Principal issues concern (*a*) the initial development and equilibration of waves in the regular steady regime, and (*b*) the nature and form of vacillatory behaviour observed in this system, with reference to their energetics, their potential vorticity dynamics and transport. Later discussion will compare the results described herein to theoretical and numerical studies of (predominantly) quasi-geostrophic processes relevant to the fully nonlinear development of baroclinic and barotropic flows.

5.1. *Initial development and equilibration*

It is conventional to describe an instability as 'baroclinic' or 'barotropic' according (*a*) to the dominant energy conversion from the zonal mean component of the flow and/or (*b*) to the direction along which the horizontal potential vorticity gradient $\partial\bar{q}/\partial r$ of the zonal mean flow changes sign (e.g. see Pedlosky 1987). In the present case, $\partial\bar{q}/\partial r$ reverses its sign in both the horizontal and vertical directions in different parts of the domain (Read 1986*b*), consistent with a $\bar{q}$-distribution consisting of a strip of negative q along the centre of the annular channel in the upper half of the annulus and a similar strip of positive q in the lower half. The initial zonal flow therefore satisfies the usual necessary (but not sufficient) condition for instability consistent with either (or both) baroclinic and/or barotropic instability. The energetics of the equilibrated steady regular flow (Read 1986*b*; Hide *et al.* 1994 – see the Appendix for definitions of the main conversion terms) suggests a mixed, though predominantly ($\sim$ 85%) baroclinic, character. By this stage, however, the flow has been substantially modified from its initial state, and it is of interest to examine whether this balance of baroclinic/barotropic character is maintained during the initial growth of the wave.

In the present work, the energetics and potential vorticity dynamics of the initial growth and equilibration can be examined using the numerical model. As outlined in §2.2, simulations were typically run by first integrating an axisymmetric version of the model to equilibrium with the required internal heating and boundary conditions. This steady balanced axisymmetric flow was then perturbed in its temperature field with a small-amplitude azimuthally wave-like disturbance, and run using the fully three-dimensional model until the wave reached equilibrium. Figure 10 shows the evolution of the azimuthal mean and non-axisymmetric components of kinetic energy (K_E and K_Z respectively) and the main conversion terms (cf. the Appendix) for K_E during the first 500 s of such a simulation of the development and equilibration of

a steady regular $m = 4$ flow at $\mathbb{B} \simeq 0.14$, $Ta \simeq 10^7$. The flow was initialized in its temperature field with a perturbation at mid-height and mid-radius comprising the superposition of a sinusoidal disturbance of amplitude 0.1 K (and $m = 4$) and a disturbance of similar amplitude applied thoughout a single azimuthal slice (at $\theta = 0$). The subsequent evolution of the flow eventually resulted in a steady regular $m = 4$ pattern.

Energetics

The initial growth of the wave components took place over the first 100–150 s of the integration, during which K_E grew by a factor $O(10^3)$ before decaying back towards its final equilibrium value via a series of damped oscillations. Meanwhile, K_Z was seen to decay, slowly at first but then more rapidly as the wave components reached their first maximum, before following damped oscillations almost in anti-phase with K_E. The main energy conversions for K_E during this period are shown in figure 10(*b*), in which it is clear that initial growth is dominated by the baroclinic conversion C_A throughout the growth period. The barotropic conversion C_K is also positive throughout this period too, though consistently smaller than C_A by a factor ~ 0.15, consistent with our earlier interpretation of the flow as predominantly baroclinic, not only in its final equilibrated state, but also throughout its initiation and growth phases. The dissipation term F_D counteracts both of the energy conversion terms throughout the growth and equilibration phases, but with a consistent phase lag, leading to a residual term which describes the net growth, transient oscillations and equilibration of K_E.

Eddy structures

The energetics of the growth phase are broadly consistent with aspects of the linear theory of wave growth in the internally heated system. It is of interest, however, to examine more closely what happens when the initial disturbance reaches finite amplitude, both during the first burst of growth and during the oscillatory equilibration. Figure 11 shows the structure of the growing eddy component at $z/D = 0.7$ in both p and T at different phases of the growth and equilibration. Significant changes in the phase structure of p' and in the overall structure of T' are clearly seen during the development of the wave, indicating that the process is not consistent with the classical quasi-exponential growth of a single normal mode, as normally postulated in idealized theoretical studies based on linear perturbation theory (e.g. Pedlosky 1987). T', in particular, undergoes an evolution from two parallel trains of wave-like disturbances, of opposite azimuthal phase on either side of the 'thermal equator' around mid-radius, towards a complex pattern of blobs and filaments which fill the domain. The rapid formation of the initial disturbance into parallel wave trains on either side of the 'thermal equator' during the very early stages of wave growth bears an intriguing resemblance to the classical 'vortex interaction' theory discussed e.g. by Lighthill (1963), Hoskins *et al.* (1985) and Schär & Davies (1990). This structure is set up remarkably quickly (within 10–20 s) from the initial disturbance (which was centred around mid-radius), but does not persist into the finite-amplitude stage, however, without some substantial modifications, indicating a strongly nonlinear phase during equilibration.

Potential vorticity

The role of nonlinear effects in the growth and equilibration of the flow is most clearly seen in the evolution of the potential vorticity in the flow. Figure 12(*a–d*) shows

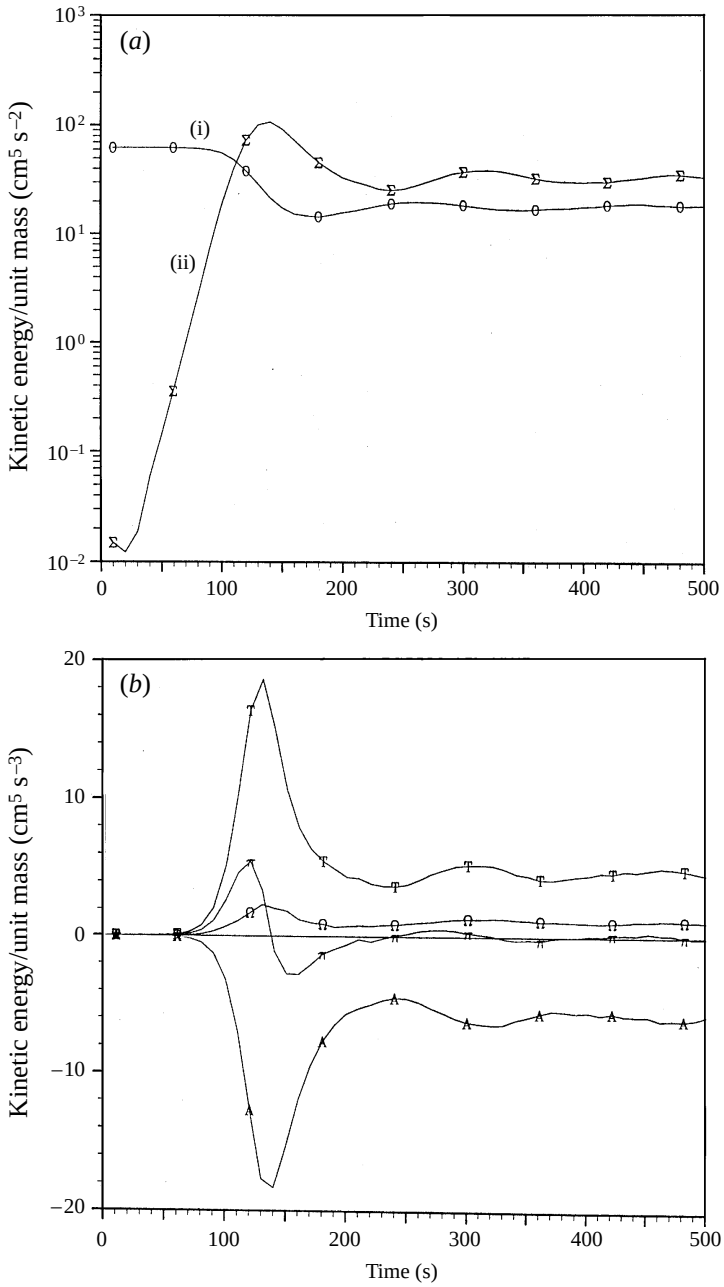

FIGURE 10. Variation of various components of the kinetic energy budget in the internally heated annulus, during the initial development of a regular $m = 4$ flow in a numerical simulation (parameters approximately as for figure 2*d*). (*a*) The variation with time of kinetic energy per unit mass in (i) the azimuthal mean ($m = 0$) and (ii) 'eddy' ($m \neq 0$) components, (*b*) the energy conversion rates for the eddy kinetic energy component. For (*b*), T denotes the baroclinic conversion rate, A viscous dissipation, Ω the barotropic wave–mean flow interaction, and the residual kinetic energy tendency is indicated by π.

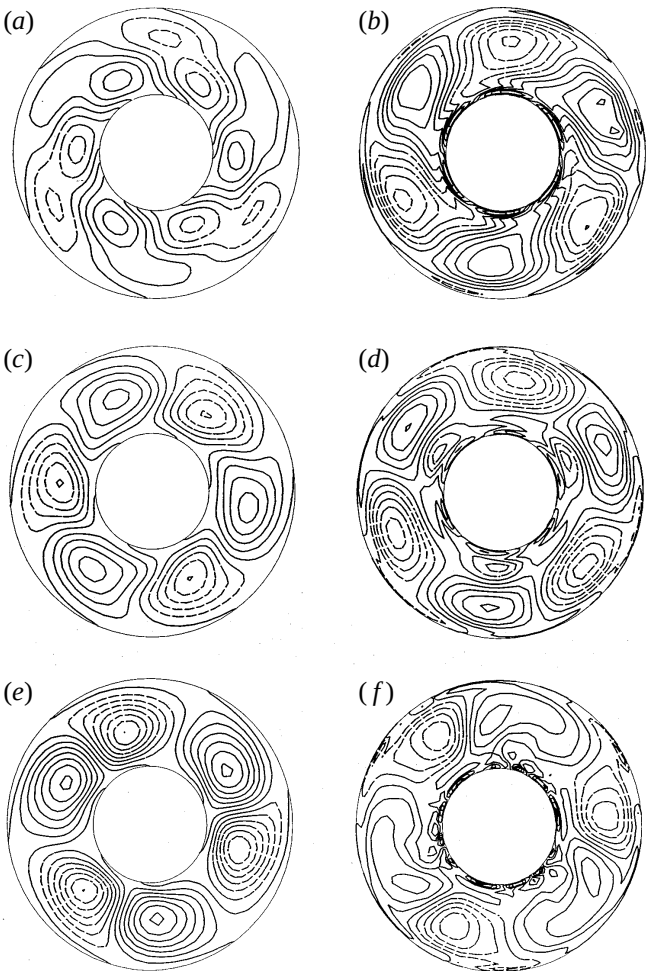

FIGURE 11. Maps of 'eddy' kinetic pressure (*a, c, e*) and temperature fields (*b, d, f*) at $z/D = 0.7$ at three stages during the initial development and final equilibration of a regular $m = 3$ flow in the internally heated annulus (parameters as for figure 2*c*): $t = 20$ s *a, b*, $t = 50$ s *c, d* and $t = 1000$ s *e, f*. Contour intervals are (*a, b*) 0.01, (*c, d*) 0.02 and (*e, f*) 0.05, in units of $\text{cm}^2\ \text{s}^{-2}$ (for pressure) and K (for temperature).

a series of maps of (quasi-geostrophic) potential vorticity, diagnosed at four different stages during the growth and equilibration phases (using the same approximations for q as Read 1985, 1988). During the first phase (figure 12*a*), the initially axisymmetric strip of q starts to undulate in response to the initial perturbation, though remains reasonably uniform along its length. At a later stage in the initial growth, just before the first peak in K_E (figure 12*b*), an azimuthally periodic varicose deformation develops, which subsequently (figure 12*c*) results in the growth and formation of a substantial pool of q of the same sign as the initial PV strip, while the strip on either side of the pool along the channel shrinks in width as it approaches the outer boundary layer. In later evolution, the pools decay slightly in amplitude, finally reaching equilibrium in the configuration shown in figure 12(*d*), in which the residual remains of the initially continuous strip of q are still visible connecting the closed

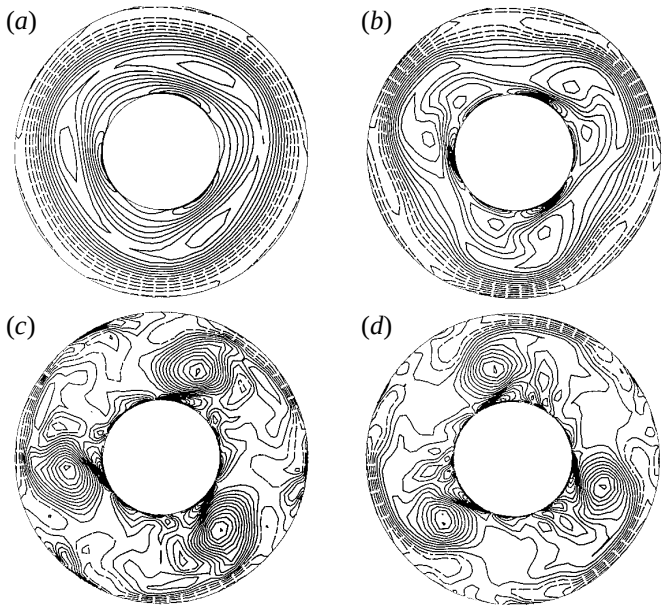

FIGURE 12. Maps of quasi-geostrophic potential vorticity at $z/D = 0.5$ at four stages during the initial development and final equilibration of a regular $m = 3$ flow in the internally heated annulus (cf. figure 11): (*a*) $t = 50$ s; (*b*) $t = 100$ s; (*c*) $t = 200$ s; (*d*) $t = 1000$ s.

pools of q, which lie at the centre of the dominant cyclonic or anticyclonic eddies (depending upon the level observed).

Relation to instability theories?

This form of highly nonlinear equilibration is quite different from the scenarios often discussed in the context of weakly nonlinear baroclinic or barotropic instability (e.g. Pedlosky 1987). The combination of both undulatory and varicose evolution during the development of compact closed eddies from an initially axisymmetric shear layer is strongly reminiscent of the behaviour found by Schär & Davies (1990) in their study of the nonlinear evolution of a mature atmospheric cold front with a 'warm precursor'. The latter leads to a low-level strip-like potential vorticity anomaly within a long trailing front, which may be idealised as a detached baroclinic shear layer (also cf. Joly & Thorpe 1990 for an analysis of the linear instability problem without thermal gradients at the ground). In the nonlinear development and equilibration, the front first undulates but then develops varicose deformations in association with the shedding of vortex filaments which roll-up into vortices of like sign to that of the vorticity of the basic zonal shear in the front. The equilibrated flow thus forms warm-cored surface cyclones, in which isolines of streamfunction and potential temperature nearly coincide in a manner indicative of a 'free-mode' character (cf. Read 1985, 1988). The energetics of the developing frontal instabilities show a strongly mixed baroclinic–barotropic character, the balance of which depends on the relative width of the front to the deformation radius (Schär & Davies 1990; Joly & Thorpe 1990). The laboratory case would seem to correspond most closely to the wider 'front 1' case of Joly & Thorpe (1990), which resulted in a predominantly baroclinic development.

As mentioned above, the initial perturbations in Schär & Davies' (1990) study also strongly resemble those in our system, with pressure perturbations which exhibit a strong zonal phase shift across the front against the prevailing shear, in association

with temperature perturbations which exhibit a $\sim \pi$ zonal phase shift across the front. Schär & Davies (1990) draw attention to the 'vortex interaction' interpretation of baroclinic and barotropic instabilities (e.g. Hoskins *et al.* 1985, following Lighthill 1963 and Bretherton 1966), in which the incipient growth of the disturbance can be viewed as the mutual interaction of two parallel trains of Rossby waves on either side of the initial front, each propagating against the prevailing zonal flow in the potential vorticity gradient on the flanks of the anomaly in the front. Growth then occurs when this interaction becomes resonant, thereby favouring cross-frontal scales of order the deformation radius or smaller. The preferred phase-locked state gives rise to the resultant structures for the growing eddies, with characteristic phase slopes in the structure of the perturbations across the potential vorticity anomaly.

The combined undulatory and varicose development of the instability in our system also seems to emulate features seen in the nonlinear development of barotropic instabilities. Pratt & Pedlosky (1991), in their numerical study of strongly nonlinear barotropic instability in geostrophic shear layers, found that the basic linear instability set the primary lengthscale of the problem, but nonlinear effects subsquently caused the flow to break up into a series of eddies or 'pools' of like-signed vorticity to that of the initial shear layer.

5.2. *Wavenumber transitions*

Once established in the regular wave regime, the typical flow pattern equilibrates as a steady symmetric wave flow which translates around the apparatus at a steady rate. On gradually changing the experimental parameters, the flow adjusts its amplitude and structure until a critical region is encountered, around which the flow may undergo a change of state e.g. to a different wavenumber, via an exchange of stability. It is of interest to compare the mode by which internally heated flows achieve this change of state with the way flows change state in the more conventional wall-heated annulus.

In the latter, it is widely observed that, as a transition to a lower wavenumber is approached (e.g. by gradually reducing Ω), the initially steady wave flow begins to undergo a periodic amplitude modulation or 'amplitude vacillation' (e.g. Pfeffer & Chiang 1967; Hide & Mason 1975; Pfeffer, Buzyna & Kung 1980; Hignett *et al.* 1985). This modulation increases in intensity as the critical parameter is approached until, at the transition point itself, the wave of wavenumber m virtually disappears at minimum amplitude, to be replaced at the subsequent regrowth of the wave by a quasi-steady pattern with wavenumber $m-1$ (e.g. see Hignett *et al.* 1985). On changing parameters in the opposite direction, however, the initially steady wavenumber-m flow undergoes a transition to a time-dependent 'structural vacillation', but retains a pattern dominated by wavenumber m to fairly extreme parameter values. Waveumber transitions are thus strongly hysteretic in the sidewall-heated system.

In the internally heated system with cooling at both sidewalls, however, the transition between wavenumbers occurs quite differently. On reducing Ω towards a transition to a lower wavenumber, the flows typically show no indication of amplitude vacillation, even very close to the transition point itself. Instead, on reaching the critical parameter value, one of the eddies in the m-wave pattern is observed to merge with one of its neighbours. Following a subsequent adjustment period, the remaining eddies modify their spacing to produce finally a regular pattern with wavenumber $m-1$. A numerical simulation of such a transition is illustrated in figure 13, which shows a (t, θ) contour map of the dynamic pressure field at mid-height and mid-radius. The flow begins with a regular $m = 4$ pattern moving in a prograde direction around the annulus. Within 300 s or so, however, the lowermost wave has merged with its

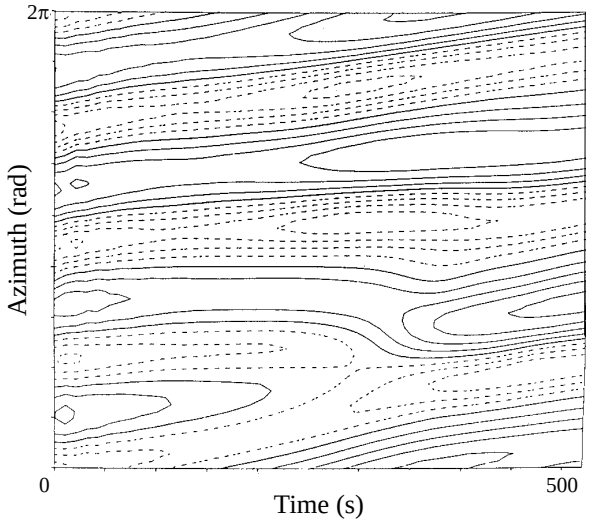

FIGURE 13. Azimuth–time map of kinetic pressure at $z/D = 0.5$ and mid-radius during a transition from $m = 4$ to $m = 3$ in a numerical simulation of baroclinic flow in the internally heated annulus; $t = 0$ corresponds to when the rotation rate was changed from 0.6 to 0.55 rad s^{-1}. Contour interval = 0.2 cm^2 s^{-2}.

neighbour, producing an initially asymmetric $m = 3$ pattern. In its later stages, the simulation shows the re-symmetrization of the flow to a regular steady $m = 3$ pattern, much as observed in the laboratory itself.

On increasing Ω towards the transition to higher wavenumbers, in contrast to the wall-heated system, the internally heated system undergoes a well-defined transition to $m+1$ via the inverse of the above process. On reaching the critical parameters, one of the eddies in the initial wavenumber-m flow is observed to split into two, and the remaining pattern then adjusts its spacing to result eventually in a regular $m+1$ flow. Such behaviour is observed until a region of 'structural/wavenumber vacillations' is encountered (see §5.3 below), which occurs in the present system around where $m = 4$ gives way to $m = 5$. It is of interest to note that Lewis (1992) also found small regions of hysteresis in his idealized quasi-geostrophic model of baroclinic flow in a straight channel, forced with a heating function analogous to the internal heating used in our experiment. That model also produced wavenumber transitions via a similar mechanism to that reported here, and did not exhibit amplitude vacillation, suggesting that such characteristics are captured within the framework of QG dynamics.

5.3. *Vacillations and transition to irregular flow*

As remarked above and in §3.1, the internally heated system differs markedly from the conventional sidewall-heated annulus in its range of time-dependent flows, especially in regard to its apparent reluctance to exhibit 'amplitude vacillation', and in the observed sequence of flow transitions towards the development of fully irregular flow and 'geostrophic turbulence'. In the latter case, the sidewall-heated annulus is observed to develop various forms of oscillation and/or localized instabilities of the basic wave structure (termed 'structural vacillation', see Hide & Mason 1975; Pfeffer *et al.* 1980; Hignett *et al.* 1985; Read *et al.* 1992) which result in relatively rapid fluctuations in the orientation and structure of the flow pattern, but which typically remains dominated by a single azimuthal wavenumber m.

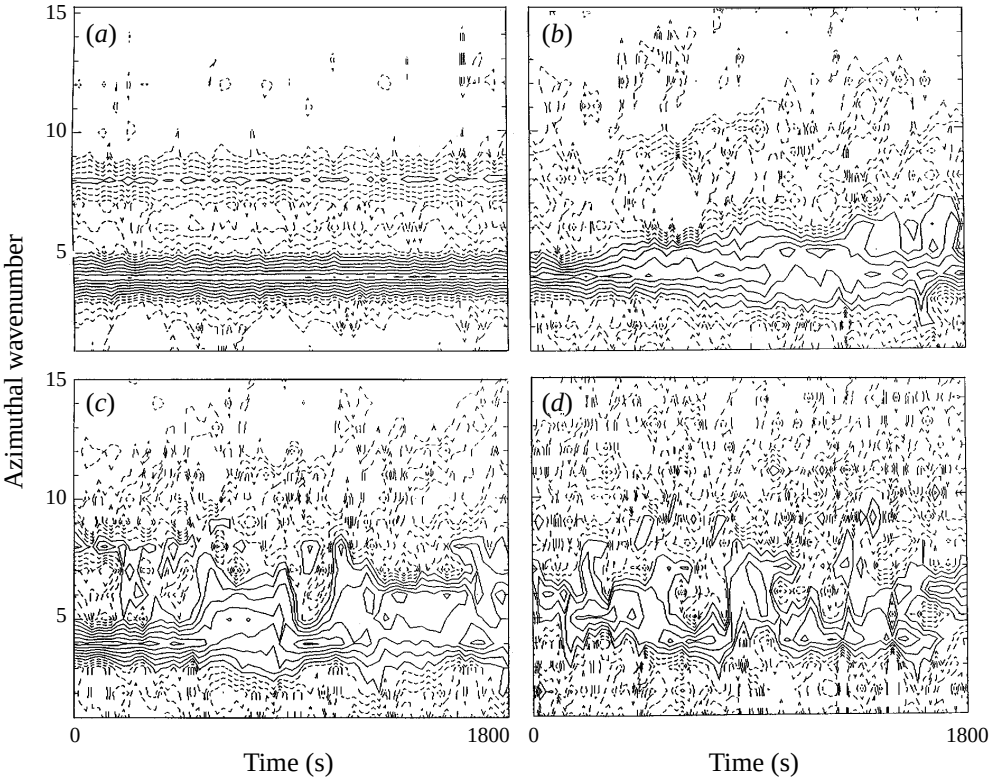

FIGURE 14. Time variations of the kinetic energy spectrum of baroclinic wave flows in the internally heated rotating annulus at various parameters spanning the transition from regular waves through WNV to irregular flow. Maps show contours of area-integrated kinetic energy per unit mass (units $cm^5\ s^{-2}$ at $z/D = 0.4$ in the azimuthal wavenumber–time plane at the following values of $\mathbb{B}$ and Ta: (*a*) 0.137 and 8.79×10^6; (*b*) 0.072 and 1.80×10^7; (*c*) 0.051 and 3.13×10^7; (*d*) 0.034 and 4.67×10^7. Logarithmic contours (to base 10) are used with an interval of 0.2, such that $\log_{10}$(kinetic energy) $\geqslant 0$ have solid contours and smaller kinetic energies are shown dashed.

In the present system, however, the onset of time-dependence as Ω is increased is typified by the tendency of individual eddy features to undergo sporadic splitting and merging events, ultimately leading to an irregular oscillation in the dominant wavenumber of the flow on timescales O(a few 10^2 s). Such behaviour may be classified as a 'wavenumber vacillation' (cf. Hide & Mason 1975) or an 'interference vacillation' involving 'wave dispersion' (cf. Pfeffer *et al.* 1980; Frueh & Read 1997), though we endeavour to distinguish between these possibilities in the results presented below. Some initial experimental results illustrating the breakdown of regular steady flow in the present system were given by Read (1993), and a similar sequence of experiments is shown in more detail in figures 14 and 15. The cases presented span the transition from steady regular $m = 4$ flow to disordered flow, the latter dominated by a range of wavenumbers $4 < m < 7$, via stages of 'wavenumber vacillation' in which the dominant wavenumber varies cyclically between $m = 4$ and $m = 5$.

The initial regular flow at $\mathbb{B} = 0.137$ (figures 14*a* and 15*a*, *d*) is clearly dominated by $m = 4$ and its azimuthal harmonics, which propagate around the annulus at a steady rate. The $m = 4$ component remains constant in amplitude to within the measurement error of around $\pm 5\%$. There is some evidence in the azimuthal

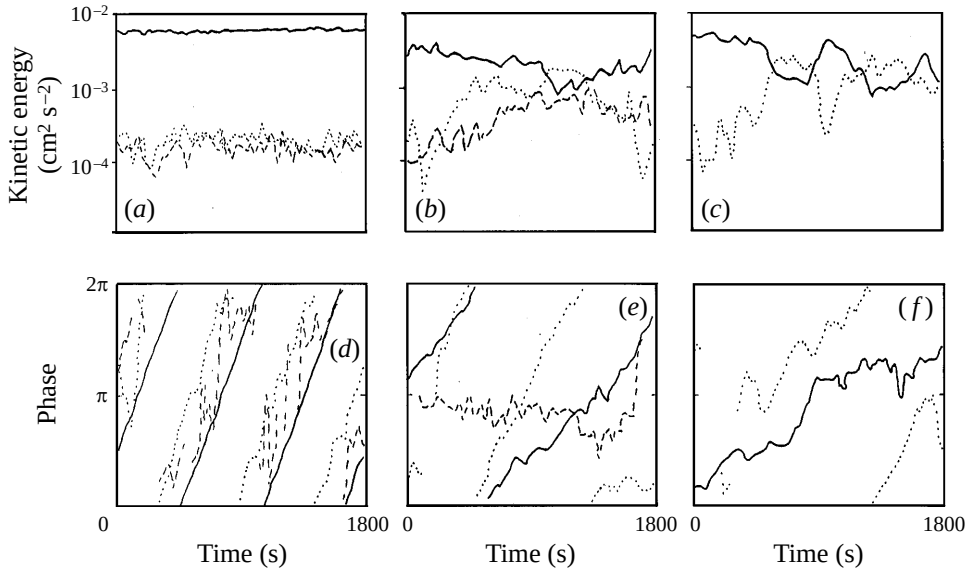

FIGURE 15. Time variation of the area-integrated kinetic energy and azimuthal phase for the $m = 3$, 4 and 5 components, derived from velocity measurements at level 2 (cf. figure 1) at three points in parameter space spanning the transition to WNV flow in the internally heated annulus. The corresponding values of $\mathbb{B}$ and Ta are: (a,d) $\mathbb{B} = 0.137$, $Ta = 8.79 \times 10^6$; (b,e) $\mathbb{B} = 0.0718$, $Ta = 1.80 \times 10^7$; and (c,f) $\mathbb{B} = 0.0508$, $Ta = 3.13 \times 10^7$.

wavenumber spectrum for significant amplitude in the adjacent sideband components $m = 3, 5$, and a suggestion that $m = 3$ and 5 are propagating with approximately the same frequency (figure 15*d*). This kind of behaviour is often observed in the sidewall-heated annulus (Hide, Mason & Plumb 1977; Read *et al.* 1992; Frueh & Read 1997), and may be indicative of a triad interaction between components of wavenumber m, $m \pm 1$ and a nearly stationary $m = 1$, possibly forced by weak departures from circular symmetry in the apparatus (cf. Hide *et al.* 1977; James, Jonas & Farnell 1981). The latter interpretation for this phenomenon is confirmed by the observation that such sideband phase locking is not observed in the idealized QG model of Lewis (1992), for which no stationary topographic features breaking the translational symmetry of the channel are present to the precision of the model numerics.

At smaller values of $\mathbb{B}$ (figures 14*b*, *c* and 15*b*, *c*, *e*, *f*), the sidebands are more prominent in the kinetic energy spectrum, as the flow begins to exhibit oscillations in the dominant wavenumber via exchanges of dominance between $m = 4$ and 5 over timescales $O(10$ min). Around $\mathbb{B} = 7.18 \times 10^{-2}$ the oscillations mainly appear as fluctuations in the spacing of the four main eddies in the flow. This appears in the kinetic energy spectrum as exchanges between $m = 4$ and 5, though the phase propagation suggests that phase locking between these two components does not generally play a role; the flow seems to act somewhat as an 'interference vacillation' in which the two competing wavenumber components pass through each other without strong nonlinear interactions, much as found in a comparable QG regime by Lewis (1992). At $\mathbb{B} = 5.08 \times 10^{-2}$, however, the fluctuations in the amplitudes of the competing components become significantly stronger ($\sim \pm 50\%$), and phase propagation shows some suggestion in the measurements (figure 15*f*) of intermittent phase locking between $m = 4$ and 5. This would seem to indicate an increased role for nonlinear wave–wave interactions in the mode competition between $m = 4$ and

5, whereas at the higher value of $\mathbb{B}$ the dynamics are, like the QG vacillating flows discussed by Lewis (1992), dominated by the wave–zonal flow interactions alone. By this stage, the character of the vacillation is much more akin to a fully nonlinear multi-pathway mode competition than a straightforward interference vacillation.

In the fully developed more irregular flow at $\mathbb{B} = 2.84 \times 10^{-2}$, the kinetic energy spectrum has broadened significantly to the extent that the flow is no longer dominated, even for short intervals, by a single wavenumber component, but exhibits a range of components between $m = 4$ and 7. Eddy merging and splitting events are common occurrences, indicating a strongly nonlinear interaction between a range of wavenumber components. Phase propagation for these various modes is rather more confused than for the earlier cases at lower values of $\mathbb{B}$, but does suggest significant intermittent correlations in phase speed between $m = 4$, 5 and (perhaps) 6 as well (though the experimental record is scarcely long enough to obtain conclusive statistics). At even smaller values of $\mathbb{B}$, the kinetic energy spectrum is observed to broaden even further in the direction of higher wavenumber, until the point is reached at which individual eddies no longer fill the annular channel in the radial direction (cf. figure 2*f*). In this regime, the flow may show a tendency to develop two or more quasi-independent trains of eddies, with strongest flow near the inner cylinder, where horizontal thermal gradients are strongest owing to the geometric effects of the cylindrical curvature.

6. Tracer transport

The principal distinction made in most theoretical discussions between vortex and wave characteristics lies in the way they advect and transport individual fluid elements within their Eulerian flow structures. Vortices are typically characterized by their tendency to trap fluid within a recirculating core for periods which are long compared to any simple eddy overturning timescale L/U. Classical wave systems, on the other hand, propagate in general at a different rate to the mass motion of the fluid itself, and individual fluid elements do not spend appreciable amounts of time in a particular region of the translating flow pattern. Lewis (1992) discussed aspects of material tracer transport kinematics within the eddy flows in his QG model analogue of the internally heated system, and found that the closed streamline regions within his steady regular flow regimes could trap material fluid elements for indefinite periods if advection is effected solely by the (horizontal) geostrophic velocity component.

In the present context, it is of interest to explore whether this QG description of material transport is valid in the realistic situation, or whether advection by the ageostrophic and/or time-dependent components of the flow permit significant 'ventilation' of the eddy cores. In this section, therefore, we describe the results of some dye tracer experiments in which a patch of dye was injected into different regions of the flow in the internally heated annulus in order to investigate the Lagrangian transport characteristics of both steady and time-dependent (quasi-periodically vacillating) baroclinic eddies.

A methyl blue dye was prepared with a density as close as possible to that of the working fluid. The dye was loaded into a remotely controlled syringe pump, mounted on the turntable. The pump was connected to a fine tube which passed through a hole in the lid of the annulus, and then into the fluid about 2 cm below the upper lid. Dye was injected into the fluid at this depth in order to avoid the Ekman boundary layer near the lid itself. The apparatus was then spun-up with steady internal heating, and allowed to settle over a period of several hours. Observations were made from

above, via the CCTV camera through the transparent lid. The dye was illuminated from below at the bottom light level, revealing the dye streak in silhouette, and the flow pattern monitored by observing the tracks of polystyrene beads which were also in suspension in the flow during the experiment.

6.1. *Steady waves*

As discussed in §3 above, regular eddies in the steady wave regime propagate slowly around the apparatus in a prograde direction, owing in part to residual potential vorticity gradients. The drift of the upper-level flow pattern was observed from particle tracking at the light level 1 and, once the point in the flow pattern at which the dye was to be injected had passed the tip of the injection line, a pulse of dye of typical duration 1–3 s was deposited into the flow. Such an interval was very short compared with the timescale for the drift of flow features past any given point, or any vacillation timescale, so the dye was effectively introduced at a single point in the flow. In the figures shown below (16 and 17), the line of dye appears as a dark curve, beginning at the source outlet at a mid-point between the inner and outer cylinders. The dye streaks persisted for around 15 min, after which time they gradually dispersed owing to the effects of diffusion. Further dye streaks could then be introduced, until the working fluid became noticeably contaminated.

Figure 16 was taken from a steady $m = 4$ flow at $\Omega = 0.997$ rad s^{-1} and $P_0 = 118$ W, close in parameter space to the flow illustrated in figures 2(*d*), 5 and 10. Figure 16(*a*, *b*) shows two images of a small dye streak introduced near the edge of the interior region of a steady drifting anticyclonic eddy. Streaks which were injected outside this point with respect to the eddy centre were rapidly sheared out along cyclonic open streamlines, outlining other eddies in the train, until lost to view when they became too fine and diffuse. In contrast, the streak shown here is trapped in the 'collar' of a typical eddy. The effects of shear dispersion within the eddy (Rhines & Young 1983) are seen to operate rapidly: the initially small spot of dye is drawn out into a fine line which follows a closed streamline and encircles the eddy in a clockwise (anticyclonic) sense. Further lateral spreading across this streakline is much slower. Occasional thicker features which appear are probably due to residual buoyancy effects, since the dye was not neutrally buoyant everywhere. Such events may lead to local spreading across streamlines, so that shear dispersion draws the dye out into further streaks parallel with the first, leading to the formation of multiple fine streaks e.g. in figure 16(*b*).

In figure 16(*b*) a second dye spot has been injected outside the trapping region in the eddies, close to the mid-point between two of the strong anticyclonic eddies in the upper levels of the flow. This spot was observed to move far more sluggishly in an anticlockwise direction, encircling the mid-point between the eddy in which the previous dye spot was released and the next eddy in the train. The relatively stagnant flow is especially apparent in the extent to which this streak is more diffuse than the fine streakline trapped in the more rapidly circulating eddy collar.

Figure 16(*c*, *d*) shows a larger spot of dye which has been released close to the centre of another eddy in the same experimental run as figure 16(*a*, *b*). As before, the spot disperses along streamlines locally to form a circular pattern, but in the more slowly rotating central region of the eddy (cf. the 'collar'). As some of the dye is slowly diffused outwards, the more rapidly circulating regions draw dye out into a finer line which develops to surround the central mass of dye (figure 16*c*). After about three minutes, however, the centre of the eddy apparently begins to clear of dye, and the dye patch slowly expands outwards into a rough ring shape. The ring showed no

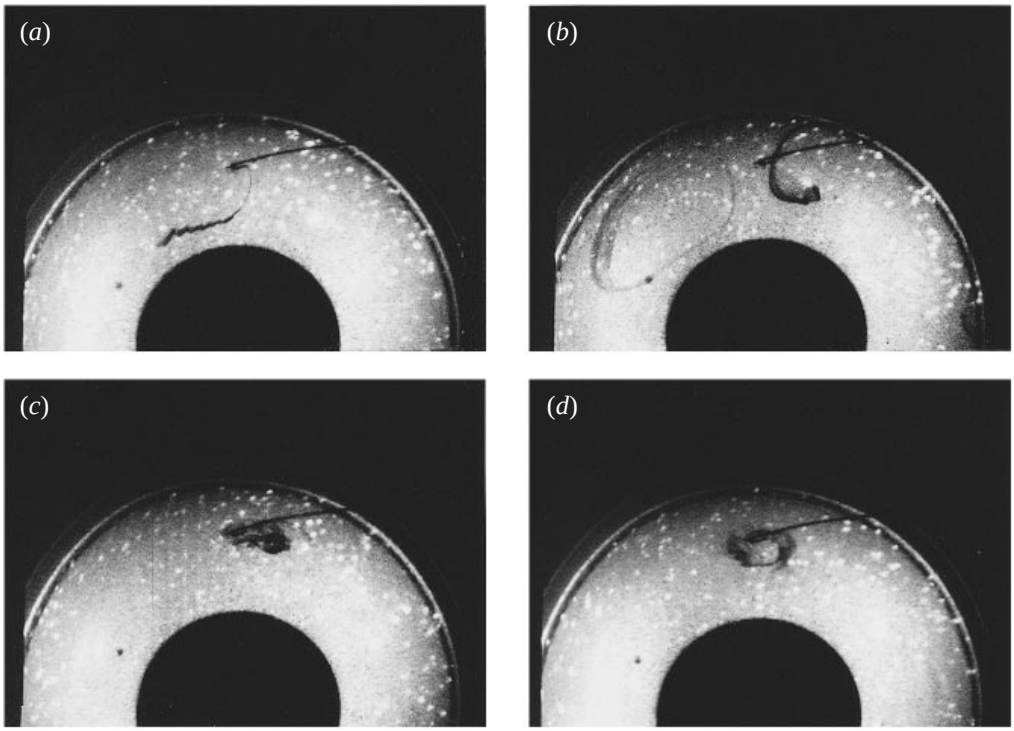

FIGURE 16. A dye streak trapped in an anticyclonic eddy in a steady $m = 4$ baroclinic eddy flow in the internally heated annulus (parameters approximately as for figure 2*d*). The streaks are injected in the collar of the eddy in (*a*) and (*b*) and a second dye spot is released prior to (*b*), showing the more sluggish cyclonic region outside the strong anticyclonic eddies. Time after initial release of dye: (*a*) 20 s; (*b*) 200 s. In (*c*) and (*d*) a dye blob was injected near the centre of an anticyclonic eddy. The blob mixes rapidly within the centre of the eddy, but is apparently later slowly expelled towards the collar. The dye remains trapped within the eddy as it propagates around the annulus until no longer visible after around 15 min. Time after dye injection: (*c*) 40 s; (*d*) 360 s.

tendency to leave the trapping region inside the eddy, but remained inside the 'collar' for a period of at least 15 min (cf. the 'advection timescale' $L/U \sim 20$ s), after which the dye became indistinct owing to molecular diffusion.

The formation of this slowly expanding ring could not be caused purely by diffusive spreading of the dye since the centre of the eddy, where most of the dye was injected, was left almost clear compared to the outer regions of the eddy. Instead it appears that the upwelling locally divergent component of the ageostrophic flow near the centre of the eddy must be acting to advect the dyed fluid outwards, though this divergent component apparently decreases in strength as the outer 'collar' is approached (since the rate of spreading then decreases). In contrast, dye streaks injected just outside the region of peak horizontal velocity in the collar of the eddies appear to suggest the presence of weakly convergent flow at these levels. As dye streaks encircle the outside edge of the eddy 'collar' a slight inward spiralling was detectable, in addition to the epicyclic motion generated by the azimuthal propagation of the eddy. The head of a streak was observed to pass inside the position of its tail from the last circuit on the leading edge of the eddy, where the propagation around the annulus would give an opposite effect were the motion great enough to be detected by this means. The combined observations imply the slow expulsion of material from the centre of each

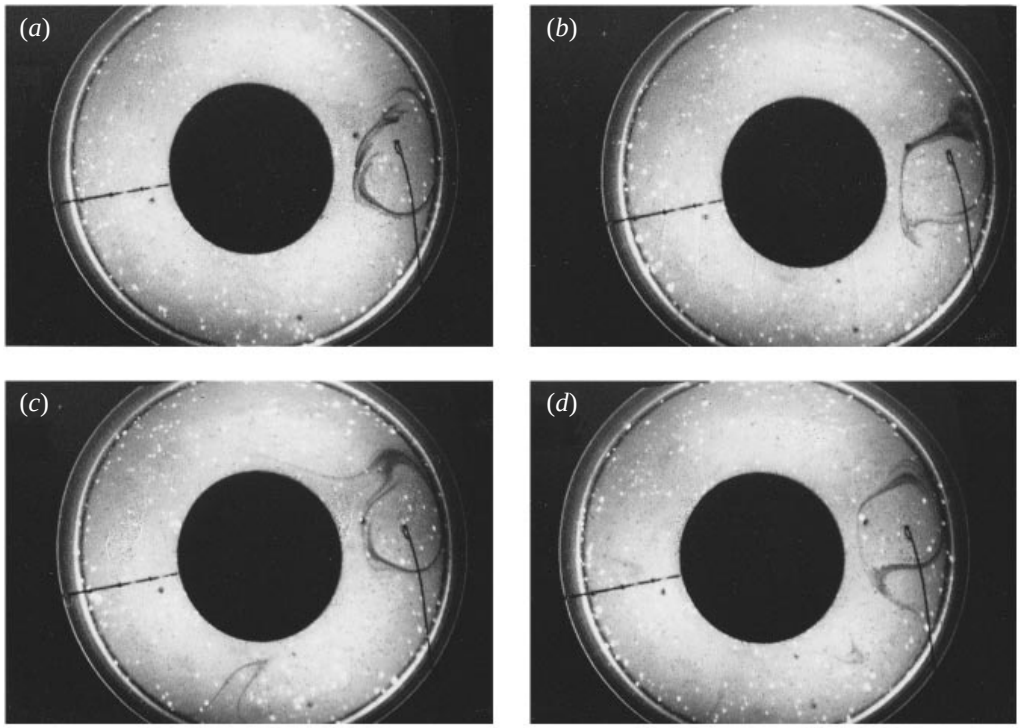

FIGURE 17. Dye streak around the collar of an anticyclonic eddy in a time-dependent $m = 4/5$WNV flow (cf. figure 2*e*), and showing loss of dye from the cusps of the eddy to the cyclonic untrapped region. Time after dye release: (*a*) 80 s; (*b*) 100 s; (*c*) 160 s; (*d*) 180 s.

eddy towards the 'collar', with streaklines spiralling slowly outwards, and with inward spiralling motion towards the 'collar' of material situated just outside.

6.2. *Time-dependent eddies*

The vortex-like trapping of fluid was clearly evident in the steady translating eddies discussed above, indicating that fluid can indeed be trapped within closed-streamline regions of the Eulerian flow structures in a frame translating with the flow pattern itself. It is of interest, however, to examine how time-dependence of the eddy structure itself and/or its wavenumber affects the transport of material within the flow. Figure 17 shows the behaviour of a dye streak injected around the collar of an anticyclonic eddy in a time-dependent flow which was undergoing quasi-periodic vacillation between azimuthal wavenumbers $m = 4$ and 5. Like the streak advected around the steady eddy in figure 16(a, b), the dye is initially drawn out by shear dispersion to surround the main eddy. However, in this case large amounts of dye are now shed at intervals through the development of strongly curved cusps at the azimuthal extremities of the eddy. In figure 17(b, c) the lost streaks move rapidly around the annulus to outline following eddies in the train. After ~ 40 s the untrapped streaks have moved around 180° in azimuth around the annulus. The lost dye was not subsequently recaptured by another eddy during the time over which it remained visible, but stayed within the freely circulating region of the flow.

In other sequences (not shown here), larger quantities of dye were injected inside the 'collar' of the anticyclonic eddies. This led to the capture of some dye inside the core of the eddy, whilst other dye escaped into the free flow outside the initial

eddy feature. This clearly demonstrated the tendency of time-dependent eddies still to trap some fluid within a central 'vortex core', while shedding material sporadically into the outer flow via sporadic cusp-shedding events. No dye was shed at other points around each eddy, which typically remained filled by a broadly homogeneous distribution of dye, only slowly diffusing beyond the 'collar'. Similar cusp-shedding events continued to occur subsequently, gradually eroding the central core until the eddy was almost emptied of dye.

The development of strongly cyclonic highly curved cusps at the periphery of each eddy is thus seen to provide a mechanism for 'ventilation' of the eddy interior at a much more rapid rate than provided by diffusion in the steady wave regime. Such shedding events arise from a local instability of the eddy structure, and have been suggested (Read 1986*b*) as a mechanism for erosion of the main eddies themselves in a form of enhanced dissipation by the erosion of the corresponding potential vorticity anomaly within each eddy core.

7. Discussion

The experimental and numerical results presented above provide a substantial amount of new information on the nature and properties of fully developed baroclinic instabilities which occur in a fluid in which the basic state comprises an extended isolated strip of potential vorticity (alternatively, in which the lateral thermal contrast changes sign). In this Section, we discuss these results in the contexts of (*a*) the validation of our numerical model against laboratory measurements, (*b*) the nature of the emerging eddies and their mutual interactions, (*c*) the extent to which QG dynamical models can represent the observed dynamics, and (*d*) implications for geophysical problems.

7.1. *Numerical model verification*

The present work has included simulations of several cases of regular steady wave flows in the internally heated system, and the initial stages of the transition towards fully irregular flow. We have thus been able to extend the application of our model well beyond the earlier work of Quon (1977) and Read (1986*a*) on the axisymmetric regime, and have carried out a quantitative validation of the kinds of simulations studied by Read (1985, 1988) in relation to the quasi-'free-mode' character of the internally heated baroclinic eddies in the steady wave regime.

The three-dimensional model is clearly seen to simulate successfully the structure and behaviour of regular wave flows in this system, both qualitatively (in the sense that the simulations favour the development of flows which closely match the flows observed in the laboratory e.g. in terms of wavenumber, types of time-dependence etc.), and quantitatively to within a few per cent, at least for the structure and amplitude of regular waves of moderate wavenumber. On performing simulations with increasing values of Ω, the numerical model did show the characteristic onset of a form of 'wavenumber vacillation' similar to that observed, though this tended to break down into highly irregular flow much more readily than in the experiment. This is likely to be a consequence of the limited spatial resolution of the simulations in this regime, for which the spread of lengthscales evidently increases rapidly as Ω is increased. In general, however, we may conclude that the model provides quantitatively successful simulations of the main elements of the regular and weakly vacillating regimes, which thus form a useful resource for the diagnosis of their dynamical properties and behaviour.

7.2. *Nature and origin of eddy flows*

The availability of complementary laboratory measurements and numerical simulations has enabled us to investigate the nature and development of large-amplitude eddies in the internally heated system in unprecedented detail. The results of numerical simulations of the development of the eddies from a weakly perturbed axisymmetric initial flow clearly show the predominantly baroclinic nature of the eddies. Starting from two parallel trains of waves on either side of the 'thermal equator', much as in the classical 'vortex interaction' scenario of Lighthill (1963), Hoskins *et al.* 1985 and Schär & Davies (1990), they evidently release potential energy in the axisymmetric flow by matching their structure closely to that of the zonal flow, concentrating baroclinic phase tilts of the appropriate sign in regions where the horizontal temperature gradient (and vertical shear) are greatest in the zonal flow. Cross-stream phase locking is also established quickly during the initial development of the flow via azimuthal adjustments of the location of each wave train, during which the overall flow develops some varicose perturbations.

A barotropic character to the flow also develops quickly during the growth of the wave. As in the development of the QG eddies in the two-layer internally heated model of Lewis (1992), the barotropic component of the growing wave mainly arises from the initial nonlinear interaction between the growing baroclinic $(m, 2)$ wave component (resulting from azimuthal phase locking across the 'thermal equator') and the $(0, 2)$ axisymmetric baroclinic flow, leading to direct barotropic exchanges of kinetic energy between the wave-like eddy and zonal flow components which typically contribute directly to sustaining the growth of the eddy itself. Meanwhile a complex network of wave–wave interactions contributes to the development of azimuthal harmonic components (although there is evidence from wavenumber-resolved energy diagnostics (James *et al.* 1981), when applied to the present flows, that lower-order harmonics are also partially sustained by direct baroclinic exchanges with the zonal flow). Despite this complex mixture of baroclinic and barotropic elements, however, it is important to note that it is the baroclinic character of the flow which dominates the nature and evolution of the growing and equilibrated eddies.

This is further manifest in the fact that the conditions under which the regular wave regime develops are uncannily similar to those favouring the regular wave regime in the sidewall-heated annulus, which itself closely matches the stability criterion for the Eady model of baroclinic instability (although the possibility that this quantitative agreement is fortuitous cannot be ruled out, e.g. see Bell & White 1988). In this respect, it is of interest to note that calculations of the linear stability boundary for zonal flows which resemble our laboratory system (Whitlow 1986), with reversing jets in both the horizontal and vertical directions, and with zero interior potential vorticity gradients, show quantitatively very close agreement with the classical Eady model in terms of critical Burger number etc.

The development of strong azimuthal harmonics in the structure of the flow also effectively concentrates the intensity of the anticyclonic branch of the growing wave (at least at upper levels, where the zonal flow has anticyclonic shear). The development of strong harmonics in the growing wave also appears to reinforce the development of varicose perturbations to the initial potential vorticity distribution, so that the emerging flow quickly develops into a chain of 'pools' of like-signed potential vorticity to that of the initial flow, linked by narrow vorticity filaments. This development is strongly akin to that observed in the barotropic numerical experiments of Pratt & Pedlosky (1991), who also performed a weakly nonlinear analysis of their system. This

analysis suggested that, although the initial growth timescale was largely set by the growth rate of the most rapidly growing linear instability, nonlinear effects resulted in explosive subsequent growth so that the varicose nature of the final equilibrated flow emerged after only a relatively small number (~ 4) of e-folding timescales. The apparent similarities between the evolution of their system and our baroclinic flow would suggest the possible value of a weakly nonlinear analysis of the equivalent baroclinic problem.

7.3. *Eddy/vortex interactions and vacillations*

Although several aspects of the structure and behaviour of the emergent baroclinic eddies in the internally heated system have many properties suggestive of a wave-like character (periodic structure in azimuth, shape-preserving translation, a self-consistent dispersion relation etc.), the development of closed 'pools' of potential vorticity in the equilibrated flow evidently also lends a degree of vortex character to the individual eddies. This manifests itself in a number of ways, including the clear trapping of fluid elements within closed eddies for long periods (as is clear in our dye-tracer experiments), and in the character of mode interactions. The clear preference for 'wavenumber vacillations' and/or 'interference vacillations' via the splitting and/or merging of individual eddies is more usually associated with coherent vortex interactions than with wave phenomena, although the amplitude/phase analyses of such 'wavenumber vacillations' suggest that the flows may also be viewed within the framework of discrete wave–mean flow interactions and/or wave–wave interactions via resonant triads.

The transition towards fully irregular flow is evidently approached via a transitional state in which two or more discrete Fourier harmonic modes (typically with adjacent wavenumbers) execute weak fluctuations in amplitude, while propagating at incommensurate phase speeds along the annular channel. The weak fluctuations would seem to be associated not with direct wave–wave interactions, but more directly via exchanges with the mean zonal flow. Such a form of 'wavenumber interference vacillation' is akin to the wave–zonal flow oscillations produced in the weakly nonlinear extension of the Eady model by Weng & Barcilon (1988). In their model, two different zonal wavenumber components competed for dominance via individual exchanges involving their nonlinear self-interactions with the zonal flow, while propagating independently, as in the present experiments, at phase speeds characteristic of the dispersion relation of the linearized problem. Such a mechanism for exchanges between wavenumbers was also evident in the QG model of Lewis (1992) in a situation more closely analogous to our experiments.

At more extreme parameter values, this transitional state leads to one in which wave–wave interactions are more significant, as evidenced by the onset of intermittent phase locking between the two principal wavenumber components. The resulting oscillations bear some resemblance to the 'triad limit cycles' of Mak (1985), which require the coherent interaction of several wavenumber components via pairs of triad interactions. However, the phase coherence between wavenumbers indicated in the experiment is at best intermittent, suggesting that coherent wave–wave interactions in the internally heated flows are relatively weak.

The apparently reduced degree of coherence between adjacent wavenumber components in the internally heated system compared with the conventional wall-heated annulus, together with the much reduced tendency for hysteresis and multiple equilibria, is strongly reminiscent of the work of Cattaneo & Hart (1990) on multiple states in the two-layer QG channel model. They noted that, for mean zonal flows with even symmetry about mid-channel, wave states occurred in distinct invariant

sets of wavenumber components with no mutual interaction between each invariant set, consistent with the occurrence of multiple stable states (depending upon initial conditions) with hysteretic transitions between them. With zonal flows which had odd symmetry about mid-channel, however, all wavenumber components were mutually accessible via nonlinear interactions from arbitrary initial conditions. The latter case would tend to favour mixed wavenumber flows, much as observed in our experiments, with little mutual hysteresis.

Cattaneo & Hart (1990) noted that their arguments strictly apply only in the rectangular channel geometry of their model, characterized by O(2) translation-reflection symmetry. In the context of the present work, however, they also suggest that similar tendencies might be observable e.g. in cylindrical systems (characterized by SO(2) symmetry), though with weak (but non-zero) interactions between the analogues of the invariant sets in the case of quasi-even symmetric zonal flows (such as in the wall-heated annulus). Such a situation would thus be expected to lead to stronger hysteresis and greater robustness of individual wave states in the wall-heated annulus than in the internally heated flows, for which the zonal flow is more closely analogous to the odd-symmetric flows of Cattaneo & Hart (1990). This tendency is certainly evident in the QG model experiments of Lewis (1992) and, as discussed above, apparently to a large extent in the experimental results presented herein. It would thus be desirable to investigate the role of domain geometry more thoroughly in the context of QG models, which can readily be integrated in cylindrical or straight channel geometry (cf. Lewis 1992; Yoshida & Hart 1986).

7.4. *Geophysical applications*

Two main areas of geophysical interest were highlighted in the introduction to this paper, as illustrations of systems where non-monotonic thermal gradients might occur in the large-scale circulation of atmospheres and oceans.

In the first case, the instability of narrow frontal zones in the atmosphere, consisting of elongated strips or filaments of potential vorticity in association with corresponding anomalies of temperature, was suggested as one possible manifestation in the Earth's atmosphere of the same kind of growth mechanism as in the present experiments. The predominance of baroclinic energetic exchanges in both systems is clearly evident, despite the highly ambiguous (mixed baroclinic/barotropic) structure of the flow, yet the scales and parameters defining the conditions under which the instability occurs seem remarkably insensitive to the flow structure. Provided the vertical lengthscale of the developing instability is appropriately defined, the preferred horizontal wavelength of the dominant disturbances is almost identical to that predicted using the classical baroclinic instability models of Eady and Charney. This clearly points to the role of the Rossby deformation radius (and the corresponding Prandtl ratio of scales) as the dominant scale in almost any form of baroclinic instability, virtually regardless of the detailed structure of the initial zonal flow state (at least in practice, if not necessarily in theory).

The preferred mode of development and evolution of the growing instability is also a common factor between the atmospheric and laboratory systems. The combination of simultaneously growing undulatory and varicose perturbations on the original zonally symmetric strip of potential vorticity is commonly seen both in numerical simulations and in actual observations, leading to the formation of closed isolated circulations which subsequently evolve in a manner which owes as much to the character of an isolated vortex as to a classical wave. Given the analogy, already pointed out, with the barotropic results of Pratt & Pedlosky (1991), this would seem

to point to an aspect of the behaviour of these systems in which the barotropic character of the flow is more clearly in evidence. The analogy with Pratt & Pedlosky (1991) suggests a need for some weakly nonlinear analysis along the lines of those authors, to see whether their arguments for the growth and equilibration timescales carry over to the baroclinic case.

The apparently paradoxical dual wave–vortex character of the internally heated baroclinic eddies in the present work has much in common also with the large stable eddies found in the atmospheres of the major planets. Many aspects of this analogy have already been extensively discussed elsewhere (Read & Hide 1983, 1984; Read 1986*b*; Hide *et al.* 1994), and will not be repeated here, except to note the extent to which the barotropic character of the flow clearly exerts some control over its mode of evolution. Such a character, even with the flows discussed above which are so clearly baroclinic from the viewpoint of their energetics, clearly emphasizes the difficulty in unravelling the true nature of the enigmatic structures on Jupiter, Saturn and Neptune. The present work also illustrates the danger of making too facile a comparison between laboratory systems subject to simple mechanical or thermal forcing on the one hand, and complex but only partially observed phenomena in nature on the other. The overwhelming majority of models and laboratory analogues put forward so far to 'explain' the giant eddies on the major planets have been fundamentally barotropic in character (e.g. Read 1994). What the present work clearly shows is that even a flow dominated energetically by baroclinic processes may behave in a way which is almost indistinguishable from a barotropic flow, at least when observed at a single altitude.

In the case of the major planets, therefore, the important next step must be to evaluate the respective roles of stratification and various thermodynamic energy sources and sinks in the atmosphere in governing the maintenance and structures of these intriguing systems. Such a problem will require ingenuity in the use of both models and new observations e.g. from the Galileo spacecraft and its successors.

It is a pleasure to thank various people who have contributed to the progress of this work over several years. Technical support in the laboratory was provided by W. D. N. Jackson and I. M. Armstrong at the Meteorological Office, and by R. D. Carter, P. Roberts and N. P. J. Thomas on numerical aspects. We would also acknowledge stimulating discussions on various matters related to this work with Drs A. A. White, P. Hignett and C. Bishop during the course of this research. Much of the earlier stages of this work was carried out with the support of the UK Meteorological Office, which is gratefully acknowledged, and S.R.L. acknowledges support received from the UK Particle Physics and Astronomy Research Council (and its predecessor, the Science and Engineering Research Council).

Appendix. Kinetic energy budgets (after Williams 1971)

In considering energy exchanges within a time-dependent flow described by the Boussinesq Navier–Stokes equations, we follow Williams (1971) in defining the azimuthal mean and eddy kinetic energies (per unit mass) within the cylindrical domain by

$$K_Z = \int_0^D \int_0^{2\pi} \int_a^b \frac{\bar{u}^2 + \bar{v}^2 + \bar{w}^2}{2} 2\pi r \, \mathrm{d}r \, \mathrm{d}\theta \, \mathrm{d}z, \tag{A 1}$$

$$K_E = \int_0^D \int_0^{2\pi} \int_a^b \frac{u'^2 + v'^2 + w'^2}{2} 2\pi r \, \mathrm{d}r \, \mathrm{d}\theta \, \mathrm{d}z. \tag{A 2}$$

For the eddy component K_E, the time evolution can be determined from the Navier–Stokes equations themselves in the form

$$\frac{\mathrm{d}K_E}{\mathrm{d}t} = C_A + C_K - F_D \tag{A 3}$$

where the conversion terms are defined by

$$C_A = \int_0^D \int_0^{2\pi} \int_a^b g\alpha w' T' 2\pi r \,\mathrm{d}r \,\mathrm{d}\theta \,\mathrm{d}z, \tag{A 4}$$

$$C_K = \int_0^D \int_0^{2\pi} \int_a^b [\boldsymbol{u}' \cdot (\bar{\boldsymbol{u}} \cdot \nabla)\boldsymbol{u}' + \boldsymbol{u}' \cdot (\boldsymbol{u}' \cdot \nabla)\bar{\boldsymbol{u}}] 2\pi r \,\mathrm{d}r \,\mathrm{d}\theta \,\mathrm{d}z, \tag{A 5}$$

and the dissipation term F_D is defined by

$$F_D = \int_0^D \int_0^{2\pi} \int_a^b \nu \boldsymbol{u}' \cdot \nabla^2 \boldsymbol{u}' 2\pi r \,\mathrm{d}r \,\mathrm{d}\theta \,\mathrm{d}z \tag{A 6}$$

where ν is the kinematic viscosity, as in table 1.

REFERENCES

Bastin, M. E. & Read, P. L. 1997 Baroclinic waves in an internally heated fluid with sloping endwalls. *J. Fluid Mech.* (in press).

Bell, M. J. 1984 The least squares method of Fourier analysing two-dimensional velocity data produced by the Video Velocity Acquisition System. *Meteorological Office, Met. O. 21 Internal Rep.* IR84/6 (unpublished).

Bell, M. J. & White, A. A. 1988 The instability of internal baroclinic jets: some analytical results. *J. Atmos. Sci.* **45**, 2571–2590.

Bretherton, F. P. 1966 Baroclinic instability and the short wave cut-off in terms of potential vorticity. *Q. J. R. Met. Soc.* **92**, 335–345.

Buzyna, G., Pfeffer, R. L. & Kung, R. 1984 Transition to geostrophic turbulence in a rotating differentially heated annulus of fluid. *J. Fluid Mech.* **145**, 377–403.

Cattaneo, F. & Hart, J. E. 1990 Multiple states for quasi-geostrophic channel flows. *Geophys. Astrophys. Fluid Dyn.* **54**, 1–33.

Craik, A. D. D. 1985 *Wave Interactions and Fluid Flows.* Cambridge University Press.

Eady, E. T. 1949 Long waves and cyclone waves. *Tellus.* **1**, 32–52.

Frueh, W.-G. & Read, P. L. 1997 Wave interactions and the transition to chaos of baroclinic waves in a thermally driven rotating annulus. *Phil. Trans. R. Soc. Lond.* A **355**, 1–53.

Gill, A. E. 1982 *Atmosphere-Ocean Dynamics.* Academic.

Hide, R. 1980 Jupiter and Saturn: giant mgnetic, rotating fluid planets. *Observatory* **100**, 182–193.

Hide, R., Lewis, S. R. & Read, P. L. 1994 Sloping convection: a paradigm for large-scale waves and eddies in planetary atmospheres? *Chaos* **4**, 135–162.

Hide, R. & Mason, P. J. 1970 Baroclinic waves in a rotating fluid subject to internal heating. *Phil. Trans. R. Soc. Lond.* A **268**, 201–232.

Hide, R. & Mason, P. J. 1975 Sloping convection in a rotating fluid. *Adv. Phys.* **24**, 47–100.

Hide, R. & Mason, P. J. 1978 On the transition between axisymmetric and non-axisymmetric flow in a rotating liquid annulus subject to a horizontal temperature gradient. *Geophys. Astrophys. Fluid Dyn.* **10**, 121–156.

Hide, R., Mason, P. J. & Plumb, R. A. 1977 Thermal convection in a rotating fluid subject to a horizontal temperature gradient: spatial and temporal characteristics of fully-developed baroclinic waves. *J. Atmos. Sci.* **34**, 930–995.

Hignett, P., White, A. A., Carter, R. D., Jackson, W. D. N. & Small, R. M. 1985 A comparison of laboratory measurements and numerical simulations of baroclinic wave flows in a rotating cylindrical annulus. *Q. J. R. Met. Soc.* **111**, 131–154.

Holton, J. R. 1989 *Introduction to Dynamic Meteorology* Academic.

Hoskins, B. J., McIntyre, M. E. & Robertson, A. W. 1985 On the use and significance of isentropic potential vorticity maps. *Q. J. R. Met. Soc.* **111**, 877–946.

Ingersoll, A. P. 1990 Atmospheric dynamics of the outer planets. *Science* **248**, 308–315.

Ingersoll, A. P. & Porco, C. C. 1978 Solar heating and internal heat flow on Jupiter. *Icarus* **35**, 27–43.

James, I. N., Jonas, P. R. & Farnell, L. 1981 A combined laboratory and numerical study of fully developed steady baroclinic waves in a cylindrical annulus. *Q. J. R. Met. Soc.* **107**, 51–78.

Joly, A. & Thorpe, A. 1990 Frontal instability generated by tropospheric potential vorticity anomalies. *Q. J. R. Met. Soc.* **116**, 525–560.

Lewis, S. R. 1992 A quasi-geostrophic numerical model of a rotating internally heated fluid. *Geophys. Astrophys. Fluid Dyn.* **65**, 31–55.

Lighthill, M. J. 1963 Boundary layer theory. In *Laminar Boundary Layers* (ed. L. Rosenhead), pp. 55–93. Oxford University Press.

Mak, M. 1985 Equilibration in nonlinear baroclinic instability. *J. Atmos. Sci.* **42**, 2764–2782.

Pedlosky, J. 1987 *Geophysical Fluid Dynamics*. Springer.

Pfeffer, R. L., Buzyna, G. & Kung, R. 1980 Time-dependent modes of behavior of thermally driven rotating fluids. *J. Atmos. Sci.* **37**, 2129–2149.

Pfeffer, R. L. & Chiang, Y. 1967 Two kinds of vacillation in rotating laboratory experiments. *Mon. Weath. Rev.* **95**, 75–82.

Pratt, L. J. & Pedlosky, J. 1991 Linear and nonlinear barotropic instability of geostrophic shear layers. *J. Fluid Mech.* **224**, 49–76.

Quon, C. 1977 Axisymmetric states of an internally heated rotating fluid. *Tellus* **29**, 83–96.

Read, P. L. 1985 Finite amplitude, neutral baroclinic eddies and mean flows in an internally heated rotating fluid: 1. numerical simulations and quasi-geostrophic "free modes". *Dyn. Atmos. Oceans* **9**, 135–207.

Read, P. L. 1986*a* Regimes of axisymmetric flow in an internally heated rotating fluid. *J. Fluid Mech.* **168**, 255–289.

Read, P. L. 1986*b* Stable, baroclinic eddies on Jupiter and Saturn: a laboratory analog and some observational tests. *Icarus* **65**, 304–334.

Read, P. L. 1986*c* Super-rotation and diffusion of axial angular momentum: I. "speed limits" for axisymmetric flow in a rotating cylindrical fluid annulus. *Q. J. R. Met. Soc.* **112**, 231–251.

Read, P. L. 1988 Finite amplitude, neutral baroclinic eddies and mean flows in an internally heated rotating fluid: 2. effects of spatially-varying N^2. *Dyn. Atmos. Oceans* **11**, 211–264.

Read, P. L. 1989 Determination of streamfunctions and velocity potentials using analysed velocity fields from VVAS data. *Meteorological Office, Met. O. 21 Internal Rep.* IR89/1.

Read, P. L. 1993 Coherent baroclinic waves in a rotating, stably-stratified fluid and transitions to disordered flow. In *Waves and Turbulence in Stably Stratified Flows* (ed. S. D. Mobbs & J. C. King), pp. 243–274. Oxford University Press.

Read, P. L. 1994 Long-lived eddies in the atmospheres of the major planets. In *Rotating Fluids in Geophysical and Industrial Situations* (ed. E. J. Hopfinger), pp. 283–299. Springer.

Read, P. L., Bell, M. J., Johnson, D. W. & Small, R. M. 1992 Quasi-periodic and chaotic flow regimes in a thermally driven rotating fluid annulus. *J. Fluid Mech.* **238**, 599–632.

Read, P. L. & Hide, R. 1983 Long-lived eddies in the laboratory and in the atmospheres of Jupiter and Saturn. *Nature* **302**, 126–129.

Read, P. L. & Hide, R. 1984 An isolated baroclinic eddy as a laboratory analogue of the Great Red Spot on Jupiter? *Nature* **308**, 45–49.

Rhines, P. B. & Young, W. R. 1983 How rapidly is a passive scalar mixed within closed streamlines. *J. Fluid Mech.* **133**, 133–145.

Schär, C. & Davies, H. C. 1990 An instability of mature cold fronts. *J. Atmos. Sci.* **47**, 929–950.

Thorncroft, C. & Hoskins, B. J. 1990 Frontal cyclogenesis. *J. Atmos. Sci.* **47**, 2317–2336.

Thorpe, A. & Clough, S. 1991 Mesoscale dynamics of cloud fronts: structures described by dropsoundings in FRONTS 87. *Q. J. R. Met. Soc.* **117**, 903–941.

Ukaji, K. 1979 Thermal and dynamical structures of convective motions in a rotating fluid annulus subject to internal heating. *J. Met. Soc. Japan* **57**, 532–547.

Weng, H.-Y. & Barcilon, A. 1988 Wavenumber transition and wavenumber vacillation in Eady-type baroclinic flows. *Q. J. R. Met. Soc.* **114**, 1253–1269.

WHITLOW, C. D. 1986 Rotating and non-rotating flows of internally heated fluids. PhD Thesis, University of Leeds, UK.

WILLIAMS, G. P. 1971 Baroclinic annulus waves. *J. Fluid Mech.* **49**, 417–449.

YOSHIDA, A. & HART, J. E. 1986 A numerical study of baroclinic chaos. *Geophys. Astrophys. Fluid Dyn.* **37**, 1–56.